

SMC-TR-93-21

AD-A267 140



AEROSPACE REPORT NO.
TR-92(2935)-17

Long Duration Exposure Facility Experiment M0003 Deintegration/Findings and Impacts

Prepared by

M. J. MESHISHNEK, S. R. GYETVAY and C. H. JAGGERS
Mechanics and Materials Technology Center
Technology Operations

15 December 1992

Prepared for

SPACE AND MISSILE SYSTEMS CENTER
AIR FORCE MATERIEL COMMAND
LOS ANGELES AIR FORCE BASE
P.O. Box 92960
Los Angeles, CA 90009-2960

Contract No. F04701-88-C-0089

DTIC
ELECTE
JUL 22 1993
S E D

Engineering and Technology Group

THE AEROSPACE CORPORATION
El Segundo, California



93 7 20 074

APPROVED FOR PUBLIC RELEASE
DISTRIBUTION UNLIMITED

93-16410




41px

This report was submitted by The Aerospace Corporation, El Segundo, CA 90245-4691, under Contract No. F04701-88-C-0089 with the Space and Missile Systems Center, P. O. Box 92960, Los Angeles, CA 90009-2960. It was reviewed and approved for The Aerospace Corporation by R. W. Fillers, Principal Director, Mechanics and Materials Technology Center. Capt. Don Johnson was the Space Test Program project officer responsible for the retrieval of LDEF.

This report has been reviewed by the Public Affairs Office (PAS) and is releasable to the National Technical Information Service (NTIS). At NTIS, it will be available to the general public, including foreign nationals.

This technical report has been reviewed and is approved for publication. Publication of this report does not constitute Air Force approval of the report's findings or conclusions. It is published only for the exchange and stimulation of ideas.


DONALD C. JOHNSON, JR.
Captain, USAF
Space Test and Experimentation Program
Customer Service Office


W. KYLE SNEDDON, Capt., USAF
MOIE Program Manager

UNCLASSIFIED

SECURITY CLASSIFICATION OF THIS PAGE

REPORT DOCUMENTATION PAGE

1a. REPORT SECURITY CLASSIFICATION Unclassified			1b. RESTRICTIVE MARKINGS		
2a. SECURITY CLASSIFICATION AUTHORITY			3. DISTRIBUTION/AVAILABILITY OF REPORT Approved for public release; distribution unlimited		
2b. DECLASSIFICATION/DOWNGRADING SCHEDULE					
4. PERFORMING ORGANIZATION REPORT NUMBER(S) TR-92(2935)-17			5. MONITORING ORGANIZATION REPORT NUMBER(S) SMC-TR-93-21		
6a. NAME OF PERFORMING ORGANIZATION The Aerospace Corporation Technology Operations		6b. OFFICE SYMBOL (if applicable)	7a. NAME OF MONITORING ORGANIZATION Space and Missile Systems Center		
6c. ADDRESS (City, State, and ZIP Code) El Segundo, CA 90245-4691			7b. ADDRESS (City, State, and ZIP Code) Los Angeles Air Force Base Los Angeles, CA 90009-2960		
8a. NAME OF FUNDING/SPONSORING ORGANIZATION		8b. OFFICE SYMBOL (if applicable)	9. PROCUREMENT INSTRUMENT IDENTIFICATION NUMBER F04701-88-C-0089		
8c. ADDRESS (City, State, and ZIP Code)			10. SOURCE OF FUNDING NUMBERS		
			PROGRAM ELEMENT NO.	PROJECT NO.	TASK NO.
					WORK UNIT ACCESSION NO.
11. TITLE (Include Security Classification) Long Duration Exposure Facility Experiment M0003 Deintegration /Findings and Impacts					
12. PERSONAL AUTHOR(S) Meshishnek, M. J., Gyetvay, S. R., and Jaggars, C. H.					
13a. TYPE OF REPORT		13b. TIME COVERED FROM _____ TO _____		14. DATE OF REPORT (Year, Month, Day) 1992 December 15	
				15. PAGE COUNT 37	
16. SUPPLEMENTARY NOTATION					
17. COSATI CODES			18. SUBJECT TERMS (Continue on reverse if necessary and identify by block number)		
FIELD	GROUP	SUB-GROUP			
			LDEF, Thermal Cycling, Atomic Oxygen		
19. ABSTRACT (Continue on reverse if necessary and identify by block number) The Aerospace Corporation Long Duration Exposure Facility (LDEF) Experiment M0003 consists of 19 subexperiments from the Aerospace Laboratories, DOD Laboratories, and contractor organizations. It was designed to study the effects of the space environment on a large variety of spacecraft materials and components, both current and developmental. The experiment was housed in four LDEF trays and contained over 1250 specimens, two data systems, and two environment exposure control canisters. Nearly identical pairs of trays were located on the leading and trailing edges of LDEF. The materials in these trays span nearly all generic functions in spacecraft such as optics, thermal control, composites, solar power, and electronics. Effects of the space environment such as vacuum, ultraviolet, atomic oxygen, meteoroid and debris, thermal cycling, and synergistic effects on various samples are described. Summaries of the on-board data are presented.					
20. DISTRIBUTION/AVAILABILITY OF ABSTRACT <input checked="" type="checkbox"/> UNCLASSIFIED/UNLIMITED <input type="checkbox"/> SAME AS RPT. <input type="checkbox"/> DTIC USERS				21. ABSTRACT SECURITY CLASSIFICATION Unclassified	
22a. NAME OF RESPONSIBLE INDIVIDUAL			22b. TELEPHONE (Include Area Code)		22c. OFFICE SYMBOL

PREFACE

The authors express their sincere appreciation to the Space Test Program (SMC/CUL), to the Strategic Defense Initiative Organization (SDIO/DTK), and to Air Force Wright Laboratory's Materials Directorate for sponsorship of this work. We would like to thank the NASA Langley LDEF Science Office for their unstinting support of our effort, and for the use of their photographs as a part of the documentation of the M0003 experiments. We also wish to acknowledge the contribution of the following individuals to this effort: Col. J. Armstrong, R. Bachus, D. H. Barker, G. W. Boyd, R. A. Brose, W. C. Burns, W. H. Childs, L. G. Clark, J. M. Coggi, A. F. DiGiacomo, L. Fishman, C. S. Hemminger, Capt. D. Johnson, J. L. Jones, 1st Lt. M. Jones, W. H. Kinard, C. Kiser, F. Knight, A. Levine, B. Lightner, N. Marquez, G. D. Martin, Lt. Col. M. Obal, L. A. Okada, R. O'Neal, K. W. Paschen, H. T. Sampson, T. A. Stoner, W. K. Stuckey, T. K. Tessensohn, G. A. To, H. E. Wang, W. Ward, D. B. Wisehart, J. C. Uht.

Accession For	
NTIS CRA&I	<input checked="" type="checkbox"/>
DTIC TAB	<input checked="" type="checkbox"/>
Unannounced	<input type="checkbox"/>
Justification	
By	
Distribution /	
Availability Codes	
Dist	Avail and/or Special
A-1	

DTIC QUALITY INSPECTED 6

CONTENTS

PREFACE	1
I. INTRODUCTION	5
II. EXPERIMENT OBJECTIVES AND DESCRIPTION	5
III. DATA SYSTEM	7
IV. EXPERIMENT OBSERVATIONS	8
A. Composite Materials	8
B. Solar Cells	9
C. Optical Samples	9
D. Thermal Control Materials	10
E. Tray Hardware	12
V. MICROMETEOROID AND DEBRIS	13
VI. CONTAMINATION	13
VII SUMMARY	14
REFERENCES	15

FIGURES

1. Diagram of leading edge 3-in. tray, D9	18
2. Diagram of trailing edge 3-in. tray, D3	18
3. Diagram of leading edge 6-in. tray, D8	19
4. Diagram of trailing edge 6-in. tray, D4	19
5. Preflight photograph of D8 tray	20
6. Preflight photograph of D9 tray	20
7. Preflight photograph of environment exposure control canister on D4, in open position	21

FIGURES (Cont'd)

8.	On-orbit photograph of D9 tray, leading edge	21
9.	On-orbit photograph of D3 and D4 trailing edge trays	22
10.	D9 tray postflight, before M0003 deintegration, in tray-holding fixture	22
11.	D3 tray postflight, before M0003 deintegration, in tray-holding fixture	23
12.	D8 tray postflight, before M0003 deintegration, in tray-holding fixture	23
13.	D4 tray postflight, before M0003 deintegration, in tray-holding fixture	24
14.	D8 (LE) canister in open position, postflight	24
15.	D4 (TE) canister in open position, postflight	25
16.	M0003 data collection sequence	25
17.	Typical orbital scan (111.3 min) data plot from conventional solar cell module	26
18.	Min/max data plot for conventional solar cell data channel	26
19.	Min/max temperature plot for graphite-epoxy LE test article	27
20.	Min/max temperature plot for graphite-aluminum composite LE test article	27
21.	Thermal cycling plot for Module III on D9 (LE) tray	28
22.	Thermal cycling plot for Module III on D3 (TE) tray	28
23.	Atomic oxygen-eroded surface of graphite-epoxy composite test article exposed on D9 (LE)	29
24.	Localized delamination of cover glass near silver weld on LE solar cell	29
25.	Typical micrometeoroid/debris damage in a solar cell cover glass	30
26.	Blistered coating damage surrounding ~1-mm dia. impact crater in LE ThF ₄ /Ag/Mo mirror test article	30
27.	Atomic oxygen erosion of aluminized Kapton radar camouflage material	31
28.	Chemglaze A276-painted sunshields flown on D4 (TE) on left and D8 (LE) on right	31
29.	SEM micrographs of surface of Chemglaze A276 paint exposed on LE (left) and TE (right)	32
30.	Response of masked Chemglaze A276 to UV radiation	32

FIGURES (Cont'd)

31.	Side-by-side comparison of LE/TE S13GLO test articles	33
32.	Signal conditioning unit (SCU) covers showing dramatic differences in damage from LE to TE.....	33
33.	Reflectance curves for S13GLO	34
34.	Micrometeoroid/debris impacts on TE EPDS sunshield	34
35.	Histogram depicting micrometeoroid/debris counts for various D4/D8 surfaces.....	35
36.	Puncture and impact crater in Chemglaze A276-painted EPDS sunshield on LE.....	35
37.	Impact crater (1.25 mm dia.) in glass test article	36
38.	Hypervelocity impact on embrittled surface of vacuum-distilled black RTV 602	36
39.	FTIR spectrum of varnish-like deposit on LE (D8) tray	37
40.	Debris contamination adhered to surface of 1.5-in. dia. silicone-based white paint test article exposed for 40 weeks in the TE (D8) canister	37

TABLES

I.	Summary of M0003 Experiments.....	16
II.	Data Channels Recorded by Data Systems	17
III.	Solar Absorptance of Thermal Control Points Retrived from LDEF	17

I. INTRODUCTION

One of the most comprehensive materials experiments on board the LDEF, M0003, was integrated by The Aerospace Corporation Mechanics and Materials Technology Center (formerly, Materials Sciences Laboratory) as principal investigator, and was designed to study the effects of the space environment on current and developmental spacecraft materials. Assembled on two leading edge (LE) and two trailing edge (TE) trays that contained over 1600 specimens, two active data systems, and two timed-exposure vacuum canisters, the experiment is a collection of 20 subexperiments from The Aerospace Corporation Laboratories, Air Force and Navy Laboratories, and Department of Defense (DoD) contractors. Many of these materials are currently in use on Space and Missile Systems Center [formerly Space Systems Division (SSD)] spacecraft.

An Industrial Advisory Group was formed to advise SSD (at that time, SAMSO) on the selection of materials for this experiment. Funding was obtained from SSD, Aerospace Mission Oriented Investigation and Experimentation (MOIE) resources, and from the DoD Space Test Program, managed by SSD/CLI. The integration of the experiment onto the LDEF and subsequent deintegration and data retrieval after the LDEF's recovery were funded by SSD/CLP. Analyses of the experiment were funded by the Strategic Defense Initiative Organization (SDIO) and the Wright Laboratory. The extended stay of the LDEF in space provided a unique opportunity to study material issues, such as longevity and space environmental stability, which bear directly on mission performance of Space and Missile Systems Center (SMC) programs.

The Aerospace Corporation, as integrating agency, was charged with documentation of the handling and disassembly of the M0003 experimental trays and with providing support to the subexperimenters. This support included full photographic documentation of the trays, modules, and quarter-modules from the earliest stages of retrieval through the complete deintegration of the trays; photographic documentation of the condition of the individual test articles; packaging and return of the test articles; and provision of flight data to the subexperimenters. Contamination of the M0003 trays was sampled and documented using nonvolatile residue (NVR) solvent wipes and tape lifts. Special attention was given to documentation of meteoroid and debris (M+D) impact phenomenology.

The four M0003 trays were disassembled in a Class 10,000 clean room facility at The Aerospace Corporation. As test articles were removed from the trays, they were individually examined, preserving the orientation of the test articles as mounted on the LDEF. They were photographed using Nomarski, bright field, and dark field optical microscopy techniques. Observations made of the condition of the M0003 test articles and of the underlying mounting hardware were compiled in an interactive data base. The data base can be sorted by subexperimenter, test article ID, material type, application, or observed damage effects. Micrometeoroid and debris damage was carefully photographed, and optical microscope surveys were performed on selected M0003 hardware items.

II. EXPERIMENT OBJECTIVES AND DESCRIPTION

The immediate objectives of this experiment were to understand the changes in the structure and properties of materials resulting from exposure to the natural space environment and to compare them to predictions based on laboratory experiments. Ideally, correlation of changes in microstructure will be made with changes in physical properties. The longer term objectives were to improve the performance and usage of existing materials and to decrease the lead times for application of new materials on DoD space systems. An important outcome from this experiment is the anticipated understanding and modeling of material degradation.

This experiment was a cooperative effort and provided the first opportunity for DoD space programs and laboratories to evaluate materials and components after long exposures to the space environment. From the original recommendations of the Industrial Advisory Group, a mix of current and developmental spacecraft materials was selected for this experiment. An overview of the material categories, the originating agency and the principal investigator is given in Table I.

The M0003 subexperimenters supplied the Aerospace principal investigator with post-flight analysis plans prior to return of their test article complements. In general, the experimental approach for most of the experimenters involved comparing preflight and postflight analyses of the specimens. Additionally, many experimenters were able to compare corresponding LE and TE test articles. For those experimenters who had test articles in the environmental exposure control canisters (EECCs), and/or reverse-mounted or shielded test articles, additional comparisons were possible. Lastly, a few experimenters retained properly stored laboratory controls for analysis and comparisons. Thus, many types of test article comparisons are possible.

The M0003 hardware consisted of four peripheral trays, two experiment power and data systems (EPDS), two EECCs, and several Li/SO₂ batteries to satisfy power requirements. The experiment was equipped to record temperature, strain, quartz crystal microbalance (QCM) frequency, solar cell output, fiber optics output, circuit interrogation, and various data system parameters. One 6-in. deep and one 3-in. deep tray connected by a wiring harness, a data system (EPDS), and a canister (EECC) were located on Rows 8 and 9 of ring D on the leading edge of the LDEF. A similar configuration was located on Rows 3 and 4 of ring D on the trailing edge. The design of the trays was modular, allowing samples to be thermally coupled or decoupled from the tray and, therefore, the LDEF structure. Over 1600 material test articles of more than 200 material types were mounted on these trays.

The layout of the trays with various sensors, primarily thermistors, also shown, is illustrated in Figures 1 through 4. Strain gauges that were used to measure the response of selected composite test articles are not shown, but were located on the reverse surface of test articles on Module III on trays D4 and D8. Twenty gauges per module were used, for a total of 40. Preflight photos of trays D8 and D9 are also shown in Figures 5 and 6. A preflight photo of the TE (D4) canister in the open position is shown in Figure 7. Trays D3 and D4 are not shown, but they were similar.

Test articles were mounted on anodized black aluminum hardware modules within the trays. Many subexperiments contained duplicate sets of test articles mounted on both the leading and trailing edge trays; a few had sets in the EECCs as well. Some subexperiments also included a set of test articles

that were mounted within the modules and were not directly exposed to the space environment. The test articles on the trays and EECCs included a variety of thermal control coatings, laser optics, composites, structural materials, laser communication components, dosimeters, antenna materials, contamination monitors, solar cells, fiber optics, and electronic piece parts.

The EECCs (on trays D4 and D8) were programmed to open in three stages, allowing varying exposures of some materials. Two weeks after the initiate signal, the canisters opened to expose a large (~3/4) area of specimens. The next canister-stepped movement occurred approximately 23 weeks after deployment and exposed another row of samples (~1/8 additional area). The final canister-stepped movement occurred at approximately 33 weeks and exposed the last row of samples (1/8 area) by opening to the canister's fullest extension. The canister drawer moved to the completely closed position at 42 weeks after initiation and remained closed during the remainder of the LDEF mission. The tape data, which will be discussed later, indicates that these programmed movements occurred properly. Thus, varying exposure times of 9, 19, and 40 weeks were accomplished for some samples, in addition to the full mission exposure of 69 months for identical test articles in other M0003 trays.

Figures 8 and 9 are representative on-orbit photographs of the M0003 trays. Several points are evident in these photos. Debris from atomic oxygen-eroded metallized Kapton radar camouflage specimens is scattered about the D9 tray. Polymer film strips, such as Kapton and silver Teflon (Ag/FEP) are broken and are projecting above the surface on both the D9 and D3 trays. Solar cells are missing on both the D3 and D9 trays due to an adhesive failure. Typical atomic oxygen (AO) erosion phenomena are apparent on the D9 tray, while UV degradation is more prevalent on the D3 tray. There is evidence of contamination due to outgassing on both trays. The painted sunshield on D4 has darkened due to UV damage, while its counterpart on D8 has remained white.

Better illustrations of the damage to the specimens are shown in the photos taken at Aerospace Corporation before deintegration of the trays. These are presented in Figures 10 through 13. This damage will be discussed in some detail later.

The canisters were opened in the clean room roughly four months after arrival of the experiment at Aerospace. Special investigation group (SIG) personnel were present during this event and had sampled the canister gases and assisted in helium leak testing of the seals. The canisters were both, essentially, at atmospheric pressure and some leakage of the front seals was detected. Photos of the opened D4 and D8 canisters are shown in Figures 14 and 15. Note the missing sample from canister D4 and erosion patterns on the stepped exposure samples on D8. Contamination patterns on the canister sides indicate the opening of the canisters by the degree of darkness of the deposits.

III. DATA SYSTEM

The data in Table II shows, in tabular form, the assignment of the various EPDS data channels on the LE (D8) and TE (D4) trays. The systems were set to run to end of tape and started scanning 2.33 hours after initiation. The scan time was set for 111.8-minute scans (1.25 orbits) every 93.16 hours. All channels were scanned five times at 3.49-minute intervals over the 111.8-minute period. An orbital scan consists of 32 points of averaged data from the five scans. The scan format is shown,

in graphic form, in Figure 16. A typical orbital plot from a solar cell string is shown in Figure 17. More informative is the minimum/maximum summary plots of the data channels. These plot the minimum and maximum values of each orbital scan for the 119 orbits for which data was collected. The corresponding min/max plot for a solar cell channel is shown in Figure 18. The plot clearly shows the orbital precession of the LDEF, which directly affects the sun exposure. Other min/max plots are given for other channels. The thermal cycling of a graphite epoxy composite specimen is depicted in Figure 19. The same cyclic variance in the data due to orbital precession of the LDEF is seen. The data indicates that the thermal performance of the LDEF and experiment M0003 were within design limits (Ref. 1). The same temperature data for a graphite aluminum composite specimen is given in Figure 20, for comparison. Higher temperatures for both min/max curves are seen, due to the lower emissivity of the aluminum relative to the epoxy. Typical thermal cycling of corresponding leading edge and trailing edge modules are shown in Figures 21 and 22. Three thermistors were used per module and they tracked quite well.

IV. EXPERIMENT OBSERVATIONS

Preliminary assessment of the M0003 experimental test articles was performed during the deintegration of the M0003 trays, using optical microscopy as the single examination tool. The objective of this nondestructive examination was to provide the subexperimenters with a quick-look summary of effects observed on their test articles that could assist them in planning their postflight investigations. The primary types of damage modes observed on the M0003 test articles were surface discolorations, atomic oxygen erosion, superficial corrosion, impact crater-formation, extraneous particulate matter adhesion to surfaces, coating microfracture-formation, and contamination residue and stain deposition. These damage modes were the result of combined effects from atomic oxygen impingement (LE only), UV radiation, thermal vacuum cycling, and outgassing contamination. Ion trails were observed on a few materials, but damage that could be attributed to proton or electron radiation was not observed on the M0003 test articles. In general, the material types on M0003 most adversely affected by the space exposure were thermal control materials, thin polymer sheets, optical mirrors, and thin film coatings. Some oxidation-sensitive metal films (notably silver) and thin polymer sheets, which were vulnerable to embrittlement and AO erosion, were almost destroyed. It should be noted that these observations are only qualitative and the in-depth investigation of the effects of the space exposure on the test articles was the prerogative of the subexperimenters, and was not the function of the deintegration team.

Many of the materials on M0003 are not considered advanced, but are in use on current satellite systems. Others are baseline materials against which performance improvements are measured. Thus, the response of these samples is important in updating the models for prediction of exposure effects and lifetime performance. A summary of performance of materials, by application, follows.

A. COMPOSITE MATERIALS

A large variety of structural composite materials was exposed on the M0003 leading and trailing edge trays. Cured and post-cured thermoplastic and thermoset resin matrices were used with low, medium, and high modulus mesophase pitch and polyacrylonitrile carbon fiber reinforcement. Some polyimide and carbon/polyimide fiber hybrid composites were also flown. Most composite constructions were either cloth laminates or varying-angle fiber wraps. The surfaces of composite

specimens on the leading edge trays were superficially oxidized and had a matte black or light gray velvety appearance, depending on their susceptibility to atomic oxygen erosion. A light ashy residue was apparent on the exposed surface of these composites. The ashy residue, if sloughed from the surface on orbit, might become a source of serious contamination, especially to optical surfaces.

Most LE composites had TE counterparts, which suffered little or no discernible damage from exposure. The most common effects noted with these materials were superficial darkening of the matrix due to UV exposure and/or discoloration of the surface due to photo-fixed contamination.

Many craters from micrometeoroid and space debris impacts were observed on these composites. The damage was confined to the immediate area of the crater on both leading and trailing edge specimens, but subsequent atomic oxygen erosion enlarged the affected area a slight amount on leading edge specimens. Typical AO damage to a composite is shown in Figure 23.

B. SOLAR CELLS

Five different types of solar cell strings (Si and GaAs cells of conventional and high efficiency design) were flown on the leading and trailing edge of the LDEF. These samples were instrumented and measurements were recorded for 14 months of exposure. The data system measured the voltage across a 0.05 Ω short circuit and the data reduction routine calculated the output current.

Examination of the cell strings after retrieval showed the cover glasses over the cells were superficially contaminated. The silver welds on the interconnects appeared intact, but localized delamination of the cover glass was apparent on some cells around the welds. Since the current measurements did not show any significant change in the performance of these cells, this degradation probably occurred after the data recording period. The damage is illustrated in Figure 24.

Coated and uncoated solar cell cover glass specimens were exposed on LE and TE trays. In addition, there were reverse-mounted controls on a TE tray, which experienced only the high vacuum and thermal conditions of the front face-mounted specimens. The cover glass coupons were mounted over Si wafers and held by Delrin retainers. The coatings included many of the UV-rejection coatings in use on present-day solar cell cover glasses. Many of the cover glasses were considerably stressed; these eventually cracked catastrophically, as did their duplicate laboratory controls. Others cracked only with exposure to the UV and atomic oxygen environments. The Delrin retainers were degraded on all of these specimens and flakes of Delrin contaminated the coating surfaces. Obviously, Delrin is not a material of choice for applications requiring resistance to AO or UV exposure on spacecraft.

Hypervelocity impacts on the cover glasses of the solar cell strings and the individual specimens produced craters surrounded by localized damage in the glass. The presence of the craters of the size found on the M0003 test articles would likely impair solar cell performance only by the obscuration of the cell across the very small area of the crater. Typical damage in a solar cell is depicted in Figure 25.

C. OPTICAL SAMPLES

Optical specimens on the M0003 trays included metal mirrors, optical solar reflectors (OSR), and dielectric-coated substrates. These materials were located on LE and TE trays, as well as in the leading and trailing edge canisters. The metallic mirrors became hazy on the leading edge trays due

to corrosion of the surface. On the trailing edge, these materials were clouded by photo-fixed contamination stains. Uncoated optical substrates were also clouded by contamination on the trailing edge, but were relatively unaffected by exposure on the LE.

Most OSR specimens were relatively unaffected by exposure, but were susceptible to contamination-staining. The exceptions were silver mirrors; both coated and uncoated versions were oxidized on the leading edge. The uncoated mirrors were oxidized beyond usefulness.

The response of dielectric-coated optical specimens depended on the materials used in the coatings. Many specimens with highly-stressed coatings became wrinkled and buckled with exposure. MgF_2 -coated fused silica substrate specimens, exposed to all environments on the M0003 trays, became crazed in every instance. Other specimen coatings suffered microcracks, but were not catastrophically damaged. The microcracking experienced by these coatings was probably due to the residual stress induced in their fabrication, as the laboratory control duplicates were also microcracked to some extent.

Hypervelocity impacts created craters surrounded by localized damage on many optical specimens. The greatest expanse of damage occurring due to impact was a 1-cm circle of blistered coating surrounding a ~1-mm diameter crater on a mirror specimen, shown in Figure 26. Coated sensors or windows that are exposed to solar UV, atomic oxygen, or micrometeoroids can experience significant optical performance degradation if the coatings are disrupted.

D. THERMAL CONTROL MATERIALS

Polymeric films, such as silver Teflon (Ag/FEP) and aluminized and bare Kapton, were eroded by atomic oxygen. Adhesive-backed Ag/FEP sheets, used as thermal protection covers over subexperiments on the M0003 trays, became milky white on both the leading and trailing edge trays. In space, the subsurface Ag reflective layer became gold-colored, perhaps due to UV-darkening of adhesive that was pressed through cracks in this layer during application of the sheets to the supporting hardware. Bare Kapton was embrittled and eroded on the LE surfaces, while Kapton coated with metal or silicone survived. The floating debris from the eroded metallized Kapton radar camouflage materials was prominent in the on-orbit photos of the M0003 LE trays (see Figure 8). Damage to the radar camouflage materials producing the Kapton debris is shown in Figure 27. Kapton was discolored on trailing edge surfaces, but remained intact. Aluminized Mylar used on adjacent LDEF trays was a serious source of extraneous debris when the Mylar was attacked by atomic oxygen, releasing very thin curls of aluminum film, which were attracted to many surfaces on the M0003 trays. Thus, for long missions or for extended exposure in low Earth orbit, the use of thin metallized polymer films is risky. Kapton specimens in the leading edge canister showed signs of erosion by AO even with only 40 weeks exposure at 250 nmi. Kapton coated with indium tin oxide did not exhibit erosion under these conditions.

Many white and black thermal control paints and coatings were exposed on M0003. Some of them were developmental, others are the common materials used on spacecraft today. More than one subexperimenter flew the same paint in his test article complement, and many had both LE and TE exposure. Some paints were also exposed in the canisters. Moreover, the EPDS sunshields and other M0003 data system sunshields were covered with white thermal control paints. These have provided large areas for M+D studies, as well as thermal control material specimens for study.

Generally, all white paints susceptible to radiation-induced color center formation were darkened by exposure to UV. These materials included those having TiO_2 , Eu_2O_3 , Al_2O_3 , and ZnO pigments. This effect was prominent on the trailing edge. However, leading edge specimens were bleached or annealed by atomic oxygen exposure (especially those containing ZnO pigments). In some cases, erosion of the UV-damaged layer restored whiteness. Aerospace Corporation subexperiment -18 exposed the white thermal control paints Chemglaze A276, S13GLO, YB-71 (ZOT) and the black paint D111, on both leading and trailing edge trays. Preliminary results on these materials are as follows.

Chemglaze A276 was used on the EPDS sunshield and is composed of TiO_2 pigment in a polyurethane binder. The solar absorptance (α_s) values measured for both leading edge and trailing edge specimens, compared to control specimens, are summarized in Table III. The dramatic difference in response of the sunshields to LDEF exposure from LE to TE is shown in Figure 28. Close examination of the paint surface indicated that the TE specimen was glossy and specular, while the LE was roughened, chalky, and full of numerous impact craters. These impact craters were surrounded by areas of blistered and peeling AO-eroded surface, pointing to preferential erosion of the organic polyurethane binder, leaving unsupported TiO_2 pigment as the surface. Scanning electron microscope photos of the TE and LE specimens that show loss of binder from the LE specimen are presented in Figure 29. Elemental analysis x-ray analysis indicates substantial loss of carbon signal from the surface of the LE specimen. As a final proof of concept, a specimen of LE EPDS sunshield paint was cut that contained a recessed bolt hole. The paint around the bolt hole had a glossy appearance where it was protected by the bolt head from AO on orbit, an indication that no erosion of the binder had occurred in that area. Response of the specimen to 500 hours of UV irradiation in a laboratory test is illustrated in Figure 30. The darkening of the specimen only in the bolt-protected area, where polyurethane binder was still present, graphically reveals that the degradation is due to UV damage to the binder. The major whitening mechanism must be AO erosion of this damaged layer.

Comparison of the α_s values in Table III leads to two major points: the lower α_s of the LE specimen relative to the control indicates loss of binder has caused an index increase or that the α_s of TiO_2 is less than TiO_2 plus binder. Oxidation of the nonstoichiometric TiO_2 could also increase its reflectivity. Also important, due to its severe susceptibility to UV degradation, Chemglaze A276 is not recommended as a white thermal control paint for spacecraft that require any significant mission lifetime.

The M0003 signal conditioning units (SCU) sunshields were painted with S13GLO and two each witness test articles were also flown on the D3 and D9 trays. Chemglaze S13GLO is a ZnO pigment encapsulated in K_2SiO_3 dispersed in a methyl silicone binder. Comparison of LE and TE specimens using either the test articles, shown in Figure 31, or specimens from the SCU covers, shown in Figure 32, dramatizes the damage to the TE paints from UV. Reflectance curves of these two samples are given in Figure 33. More important, the roughly 300% increase in α_s from control to TE is not in line with predictions from ground test results (Refs. 2 and 3). These specimens are still under investigation, but microscopy and surface analysis have not indicated detectable erosion of the material. It is believed that the UV-induced color centers formed by oxygen vacancies on the trailing edge are oxidized or annealed on the leading edge by AO. This mechanism is still under investigation. Response of S13GLO to AO and UV is important since this tends to be the paint of choice for many SMC programs because of its ease of application, low cost, low α_e , and flexibility.

The white paint, YB-71, which is Zn_2TiO_4 pigment in K_2SiO_3 binder commonly called "ZOT", demonstrated marked stability towards both AO and UV relative to the other white paints previously discussed. In Table III a slight degradation of α_s identical for LE and TE specimens, presumably due to UV, is shown. Interestingly, some ZOT specimens formed crystalline whiskers in the K_2SiO_3 binder. Leading edge specimens are not whiter than the TE specimens, indicating that bleaching or annealing of color centers is not a dominant mechanism in this material--for unknown reasons. Due to its UV stability, ZOT may be a good choice for LEO spacecraft. However, its stability towards electron/proton radiation is in doubt and may render it less effective at geosynchronous or elliptical orbits.

The D111 black thermal control paint, which consists of bone black in K_2SiO_3 binder, was essentially unaffected by AO, but some decrease in absorptance was measured relative to the TE specimen. Another black paint, Chemglaze Z306, which has a polyurethane binder, sustained more severe degradation than D111. Most of the LDEF hardware was painted on the reverse surface with Chemglaze Z306. The properties of these paints are still under investigation. Other thermal control paints and coatings such as black anodized aluminum, used extensively on the M0003 test article mounting hardware, were bleached by UV exposure.

E. TRAY HARDWARE

General observations and results of the examination M0003 hardware are as follows.

Extensive contamination deposits as a result of outgassing, contamination, and UV-photolyzed reaction are seen on the M0003 trays. The synergism between outgassing and UV is striking. This phenomenon of enhanced photodeposition needs to be taken into account in modeling, ground testing, and material qualification.

There were significant adhesive failures on M0003. Some adhesives (the RTVs) that are commonly used to bond Kapton to Ag/FEP debonded as did acrylic adhesives bonding solar cells. The issue of adhesive performance as a function of thermal cycling and UV exposure poses a genuine concern for spacecraft in LEO and better (longer) testing and qualification is required.

Fasteners on LDEF and M0003 do not lend themselves to obvious interpretation of their performance. We have observed backed-out bolts, loose bolts, frozen bolts, and broken bolts on both the leading and trailing edges. Some bolts, which were relatively loose, tightened or galled on removal. The 1500 fasteners that were documented on M0003 during removal have been put into a data base for study. Clearly, fastener performance will be a major issue for any system requiring longevity and/or maintenance in space.

For M0003, there is good news for electrical connectors, solder joints, wires, mechanisms, batteries, motors, tape recorders, and computers. No significant anomalies were noted on orbit. Inspection also showed good performance and integrity after retrieval. No significant outgassing of electronic parts was observed. An early and perhaps risky conclusion is that all the costs and effort put into reliability of electrical devices is overdone. There were devices on our experiment that were commercially obtained and performed flawlessly.

V. MICROMETEOROID AND DEBRIS

During the deintegration of the M0003 experiment, there was an opportunity to observe and photograph impacts in several types of materials. In addition, trays D4 and D8 contained sunshields and instrument covers that provide large areas (2/3 of trays D4 and D8) for debris studies. These were meticulously examined and all hypervelocity impacts 0.1 mm in diameter or larger were charted. A computer-generated map of one of these surfaces is shown in Figure 34. A histogram that summarizes the meteoroid and debris counts to date is displayed in Figure 35. This data is currently being compared to existing meteoroid and debris models. Figures 36 through 38 are photographs illustrating typical impact phenomenology in various materials. While none of the damage should be considered as catastrophic, its effect on mission performance must be carefully evaluated. Interesting reaction zones are seen on some of these impact features, although they are not well understood at this time.

VI. CONTAMINATION

Contamination from outgassing and particulates was legion on M0003. This was documented extensively through photography and sampled by means of solvent wipes and tape lifts. These were taken prior to and during disassembly. Optical and SEM photos were used to analyze the tape lifts, while Fourier Transform Infrared (FTIR) spectroscopy was used to analyze the contamination films. This work is still in progress.

Heavy varnish-like deposits were found on the trays, the thickest being on D8 and D9. Flow patterns were observed which suggested that the origin of the outgassing was from within the LDEF structure. FTIR analysis of this residue is shown in Figure 39. Bands present in the spectrum suggest it is made up of hydrocarbons, urethanes, and silicones.

Ultraviolet photolysis and AO altered the contamination on both leading and trailing edges. On the trailing edge, UV has darkened and photo-fixed the deposits. The same occurred on the leading edge; however, near the end of the LDEF mission, the higher AO concentration at lower altitude oxidatively removed some contamination. Silicone layers were oxidized to form a silicate or silica deposit. Thus, much of the contamination was covered with glassy-type coatings and could not be removed by solvent wipes. These synergistic effects of UV and contamination and AO and contamination (Refs. 4 and 5) have been investigated previously. More work needs to be done in this area to quantify these effects. Chemglaze Z306, applied to the interior of the LDEF, is considered a likely source of much of this contamination.

Particulate contamination on individual test articles could be identified as originating from deteriorated nearby materials on M0003 and other LDEF trays. Debris found on test articles flown in the canisters, particularly fibrous debris (Figure 40), may have come from the shuttle payload bay covers.

VII. SUMMARY

The most significant results from LDEF/M0003, the subsequent lessons learned, and impacts are presented below, together with recommendations for future work.

Micrometeoroid and debris impacts on M0003 were numerous; however, none caused catastrophic damage. Nevertheless, the size and number of such impacts raise serious concerns regarding the escalating amount of space debris. Damage to a system (especially optics) resulting in loss of mission performance needs to be carefully evaluated and modeled, not only with respect to collision probabilities, but also to impact phenomenology.

Contamination on LDEF/M0003 was more pronounced and severe than expected and points to excessive outgassing from multiple sources. Examination of hardware surfaces indicates that outgassing occurred well into the LDEF mission and that venting from the interior of LDEF was a major source. Clearly, there is a need for cleaner spacecraft and better modeling of contamination transport. Contamination control should be made part of spacecraft design. Of particular note is the ubiquitous UV photolysis of contaminant deposits, as well as the alteration (oxidation) of such deposits by atomic oxygen. The synergistic effects of these three phenomena need to be better understood and modeled.

The degradation of some paints, coatings, and films was significantly greater than expected. The threefold increase in α_s of S13GLO, the crazing of MgF_2 , and the erosion of Ag/FEP, all point to a need for better correlation of ground and flight test data, and better test methods. The significant number of adhesive failures raises the issue that longer testing is required to evaluate the effects of repeated thermal cycling on adhesive performance.

Synergistic effects are emerging as the most important and interesting phenomena; specifically the combined effects of AO and UV radiation on materials and contamination; reactions of AO and UV at debris impact sites; and the effects of UV and thermal cycling on materials, particularly polymers.

On the positive side, electrical and mechanical systems exhibited little or no anomalies. It would seem that much of the degradation of materials, especially from AO, is superficial and not a significant problem. This is especially true for structures and composites having any appreciable thickness.

REFERENCES

1. W. M. Berrios, *Long Duration Exposure Facility Post-Flight Thermal Analysis, Orbital/Thermal Environment Data Package*, NASA Langley Research Center, Hampton, VA (3 October 1990).
2. G. A. Zerlaut, J. E. Gilligan, and N. A. Ashford, *Space Radiation Environmental Effects in Reactively Encapsulated Zinc Orthotitanates and Their Paints*, AIAA paper No. 71-449, Tullahoma, TN (24-28 April 1971).
3. R. J. Mell, and Y. Harada, *Space Stable Thermal Control Coatings*, Wright Laboratories Materials Report, AFWAL-TR-87-4010, Wright Research and Development Center, Dayton, OH (May 1987).
4. H. S. Judeikis, G. S. Arnold, M. M. Hill, R. C. Young Owl, and D. F. Hall, "Design of a Laboratory Study of Contaminant Film Darkening in Space," Vol. 1165, *Scatter from Optical Components*, Society of Photo-Optical Instrumentation Engineers, San Diego, CA (1989).
5. M. J. Meshishnek, W. K. Stuckey, J. S. Evangelides, L. A. Feldman, R. V. Peterson, G. S. Arnold, and D. R. Peplinski, *Effects on Advanced Materials: Results of the STS 8 EOIM Experiment*, Atomic Oxygen Effect Measurements for Shuttle Missions STS 8 and 41G, Vol. II, NASA Technical Memorandum 100459, Goddard Space Flight Center, Greenbelt, MD (September 1988).

Table I. Summary of M0003 Experiments

Sub-experiment Number	Scope	Experimenter	Agency
-1	Radar camouflage materials and electro-optical signature coatings	Charles Hurley	Univ. of Dayton Research Inst. 300 College Park Dayton, OH 45469-0001
-2	Laser optics	Linda De Hainaut	Phillips Lab/LIDA Kirtland AFB, NM 87117-6008
-3	Structural materials	Charles Miglionico	Phillips Lab/PL/VTSI Kirtland AFB, NM 87117-6008
-4	Solar power components	Terry Trumble	Wright Labs/POOC Wright Patterson AFB, OH 45433-6533
-5	Thermal control materials	Charles Hurley	Univ. of Dayton Research Inst. 300 College Park Dayton, OH 45469-0001
-6	Laser communication components	Randall R. Hodgson	McDonnell Douglas Astronautics Corp. Mail Code 1067267 P. O. Box 516 St. Louis, MO 63166
-7	Laser mirror coatings	Terry M. Donovan	3481 Murdoch Dr. Palo Alto, CA 94306
-8	Composite materials, electronic piece parts, fiber optics	Gary Pippin	Boeing Aerospace Co. Materials Technology Dept., MS 2E-01 P. O. Box 3999 Seattle, WA 98124
-9	Thermal control materials, antenna materials, composite materials, and cold welding	Brian C. Petrie	Lockheed Missiles and Space Co. Dept. 62-92, Bldg. 564 P. O. Box 104 Sunnyvale, CA 94086
-10	Advanced composite materials	Gary L. Steckel	The Aerospace Corporation P. O. Box 92957, M2/242 Los Angeles, CA 90009
-11, -12	Contamination monitoring Radiation measurements	Eugene N. Borson	The Aerospace Corporation M2/272
-13	Laser hardened materials	Randall R. Hodgson	McDonnell Douglas Astronautics Corp. Mail Code 1067267 P. O. Box 516 St. Louis, MO 63166
-14	Quartz crystal microbalance	Donald A. Wallace	QCM Research 2825 Laguna Canyon Road P. O. Box 277 Laguna Beach, CA 92652
-15	Thermal control materials	Oscar Esquivel	The Aerospace Corporation M2/241
-16	Advanced composites	Gary L. Steckel	The Aerospace Corporation M2/242
-17	Radiation dosimetry	Sam S. Imamoto, J. Bernard Blake	The Aerospace Corporation M2/260
-18	Thermal control paints	Christopher H. Jagers	The Aerospace Corporation M2/272
-19	Electronic piece parts	Seymour Feuerstein	The Aerospace Corporation M2/244
-20	Tray hardware	Michael J. Meshishnek	The Aerospace Corporation M2/271

Table II. Data Channels Recorded by Data System

	Leading Edge	Trailing Edge
Temperature	31	32
Strain	20	20
Solar Module Output	6	6
Quartz Crystal Microbalance	1	1
Fiber Optics	1	-
Circuit Interrogation	1	-
	Number of Instrumentation Monitor Channels	
DCPA/EPDS		
Voltage	2	2
Current	1	1
Temperature	1	1
Signal Conditioning Unit Temperature	2	2

Table III. Solar Absorptance of Thermal Control Paints Retrieved from LDEF

Material	Position	Solar Absorptance, α_s	
		Test Article	Lab. Control
A276	Leading Edge	0.228	0.282
	Trailing Edge	0.552	
YB-71 (ZOT)	Leading Edge	0.182	0.130
	Trailing Edge	0.182	
S13GLO	Leading Edge	0.232	0.147
	Leading Edge	0.228	
	Trailing Edge	0.458	
	Trailing Edge	0.473	
D-111	Leading Edge	0.933	0.971
	Trailing Edge	0.968	

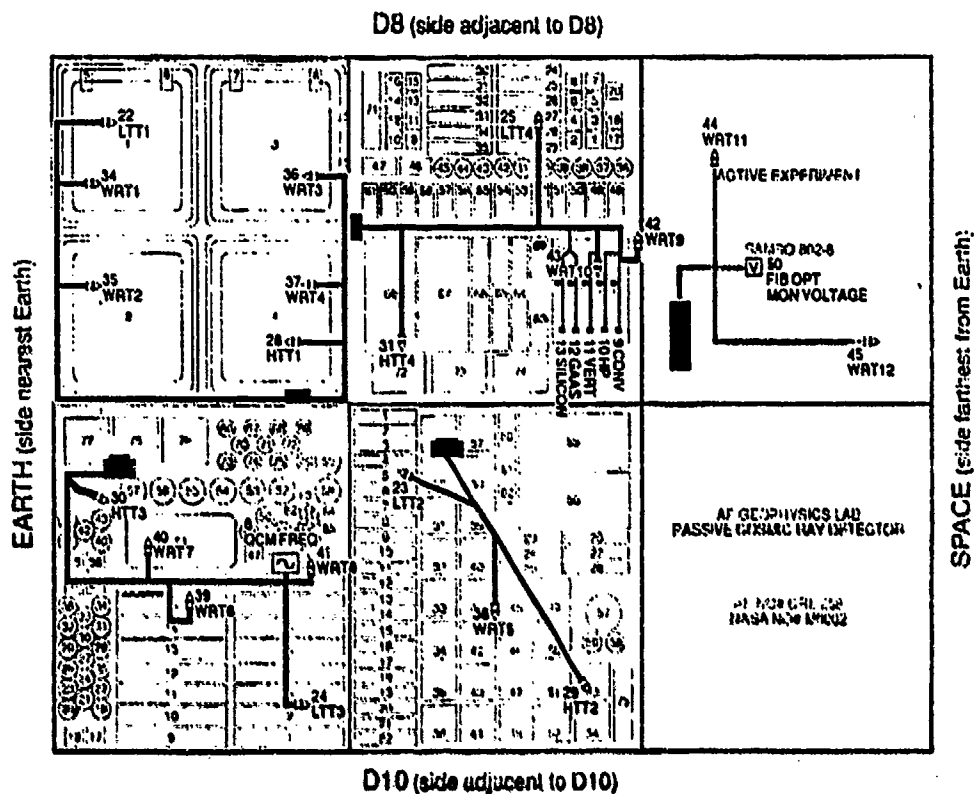


Figure 1. Diagram of leading edge 3-in. tray, D9

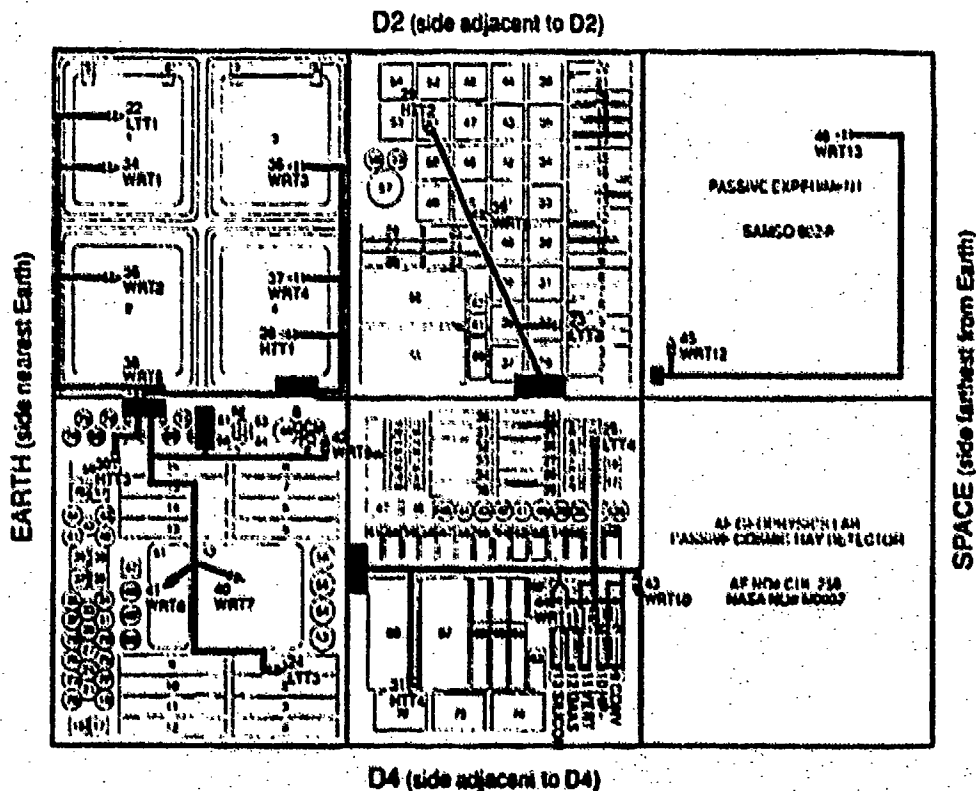


Figure 2. Diagram of trailing edge 3-in. tray, D3

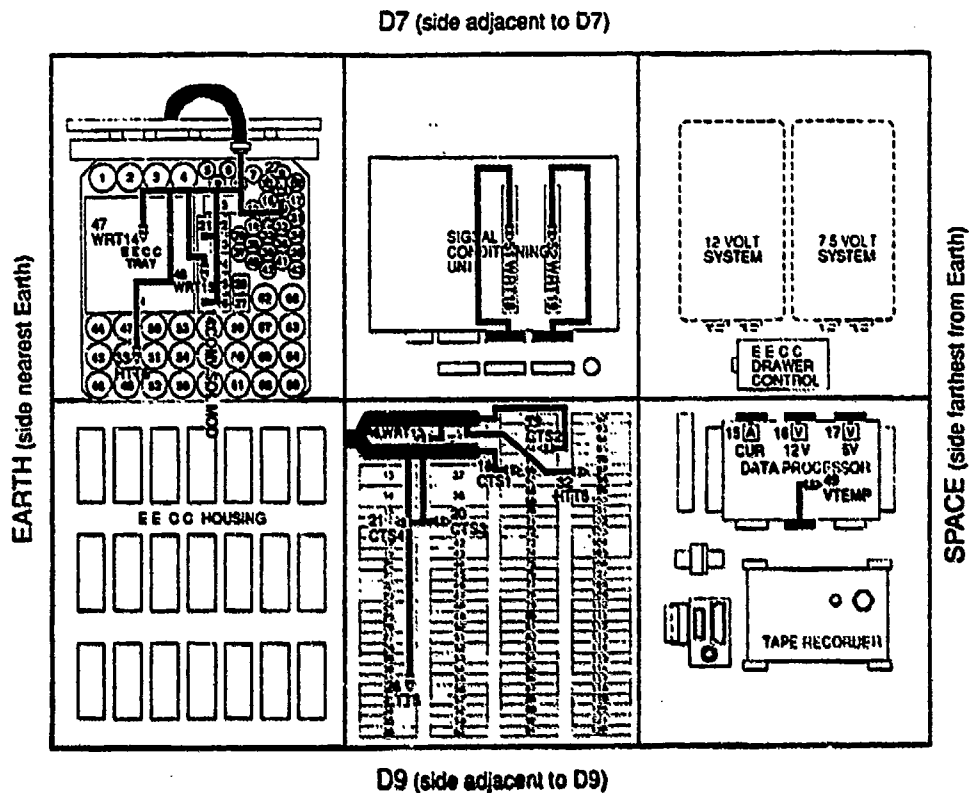


Figure 3. Diagram of leading edge 6-in. tray, D8

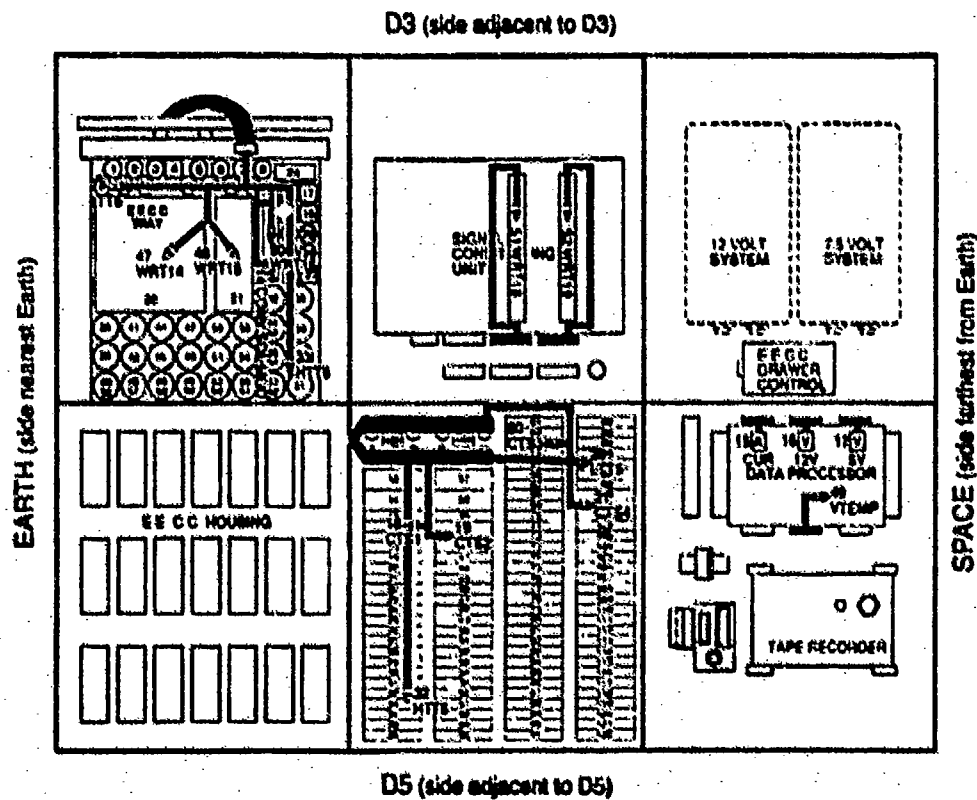


Figure 4. Diagram of trailing edge 6-in. tray, D4

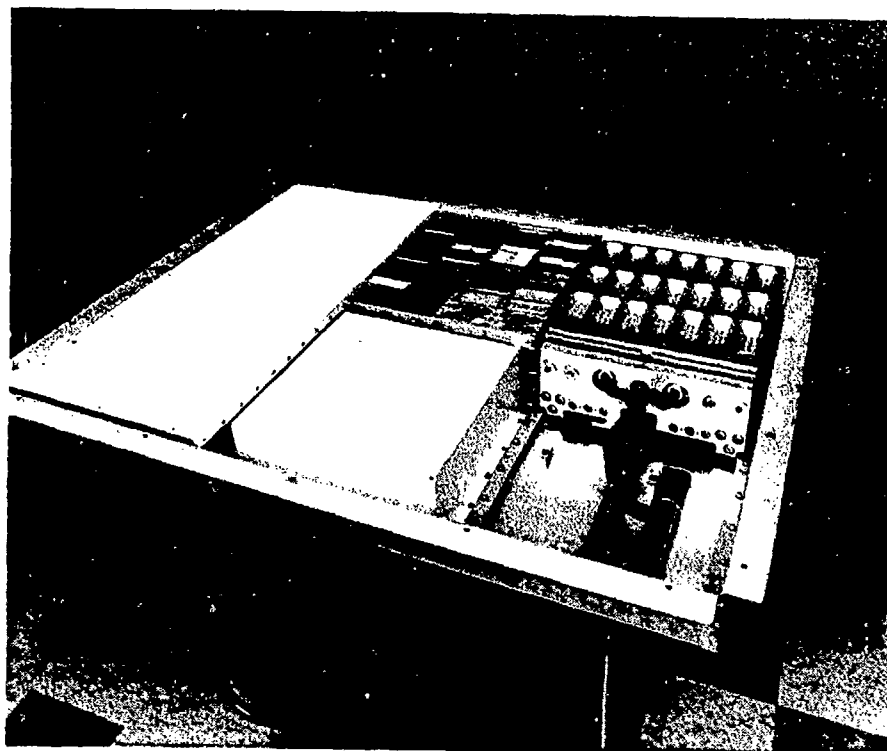


Figure 5. Preflight photograph of D8 tray

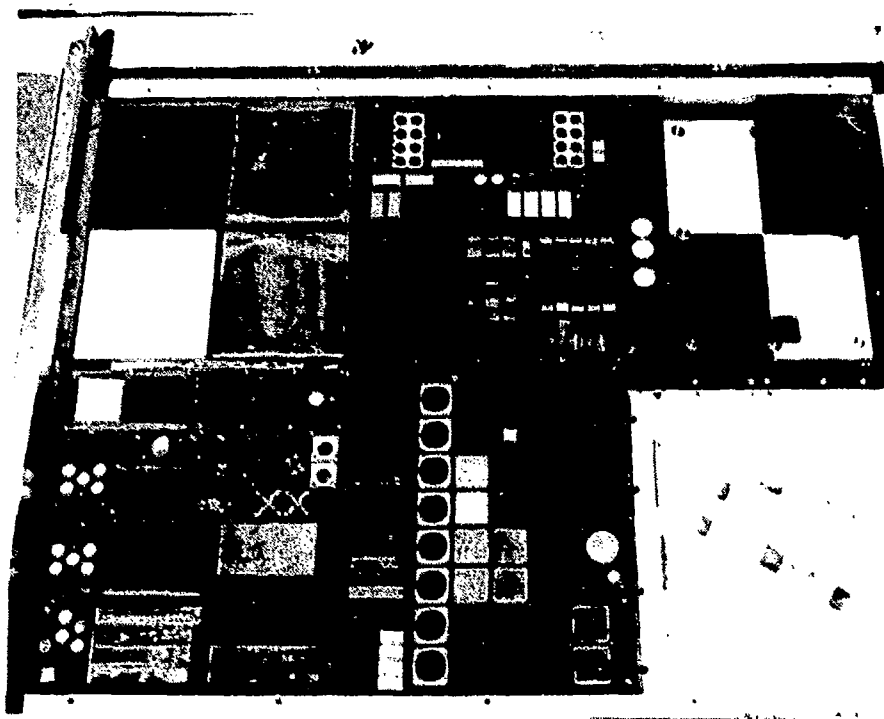


Figure 6. Preflight photograph of D9 tray

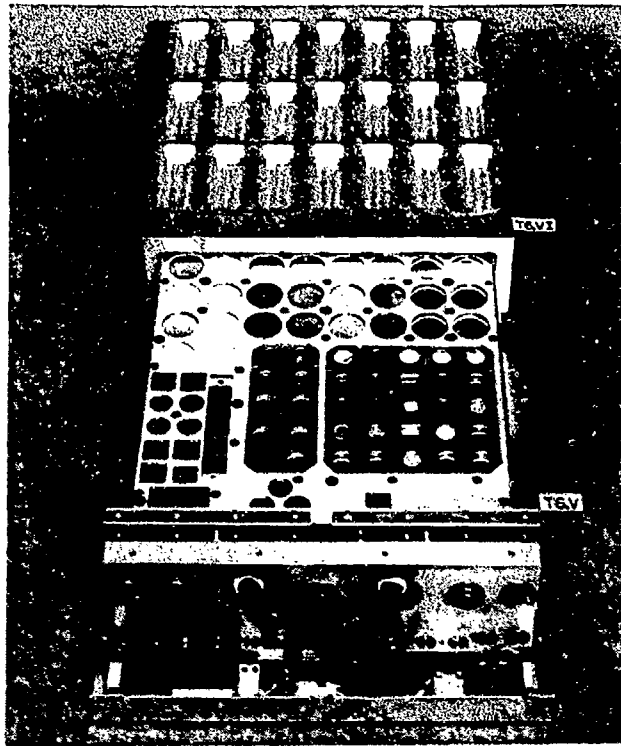


Figure 7. Preflight photograph of environment exposure control canister on D4 in open position

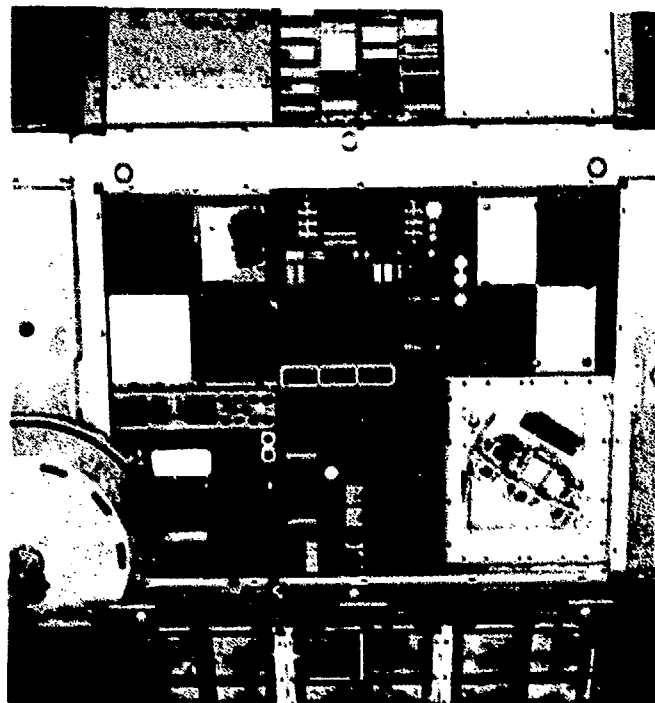


Figure 8. On-orbit photograph of D9 tray, leading edge. Note the debris above the surface from AO-deteriorated materials on the tray

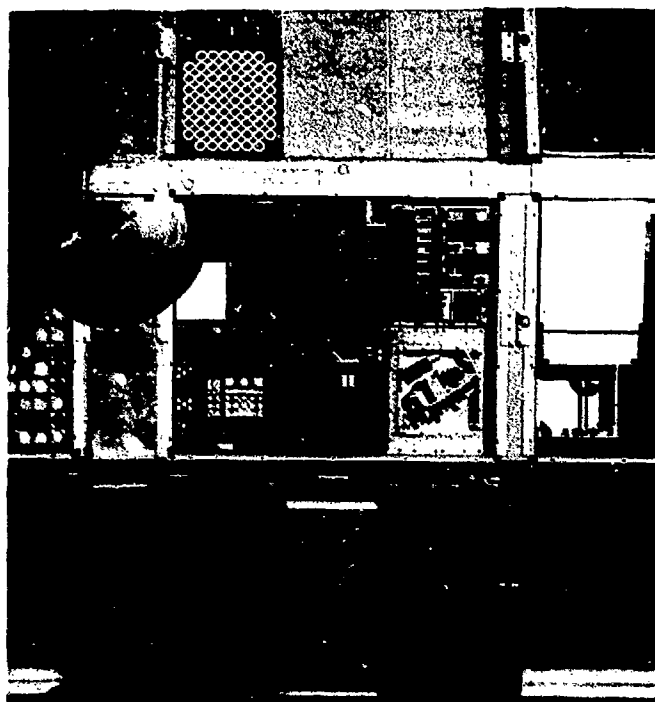


Figure 9. On-orbit photograph of D3 and D4 trailing edge trays. Most noticeable effects are contamination-staining and darkening of white paint coatings

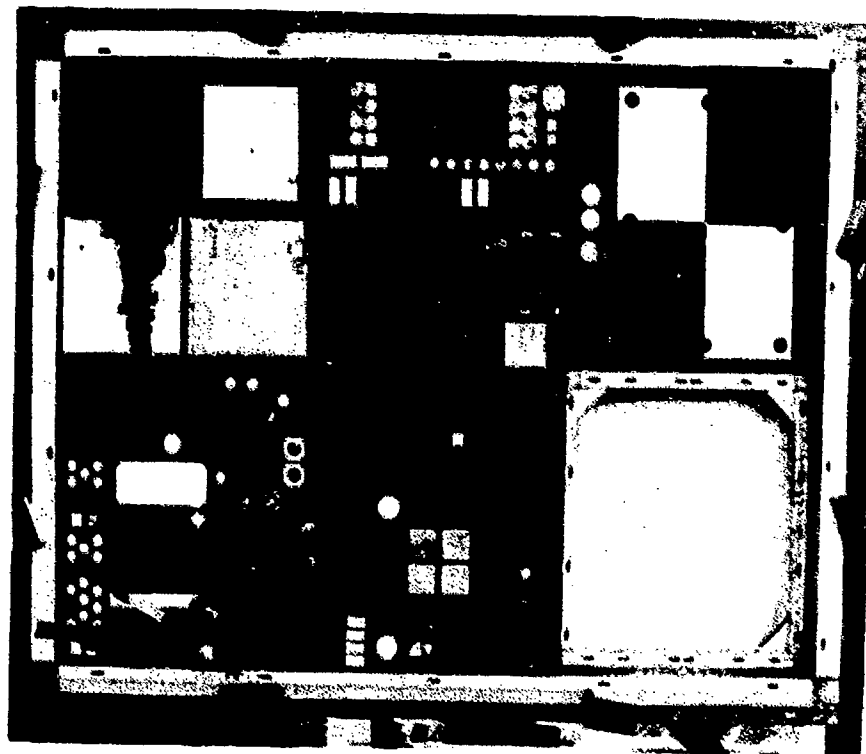


Figure 10. D9 tray postflight, before M0003 deintegration, in tray-holding fixture

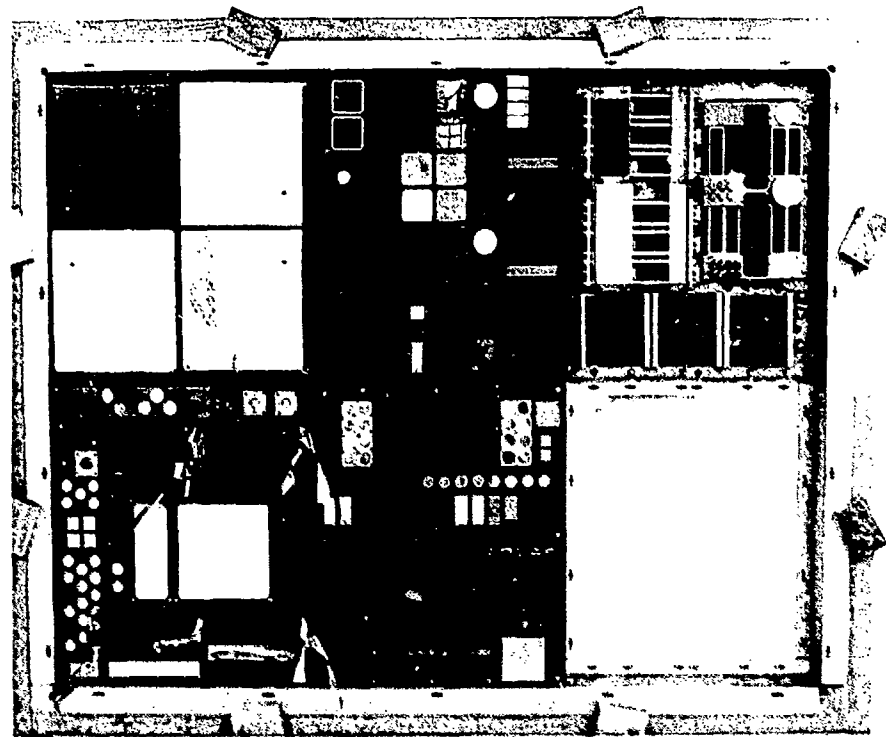


Figure 11. D3 tray postflight, before M0003 deintegration, in tray-holding fixture

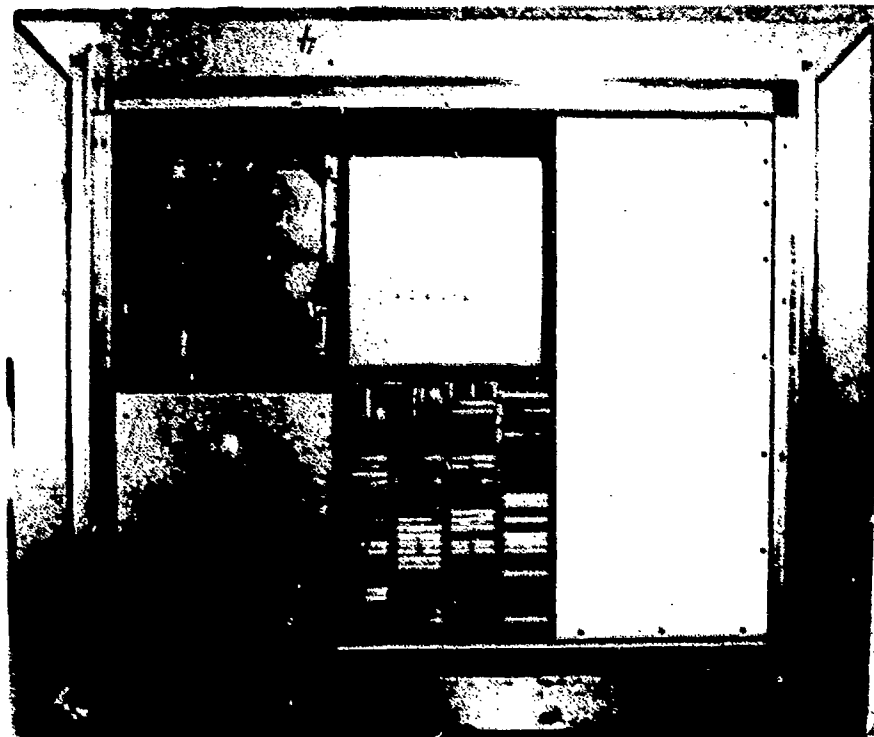


Figure 12. D8 tray postflight, before M0003 deintegration, in tray-holding fixture

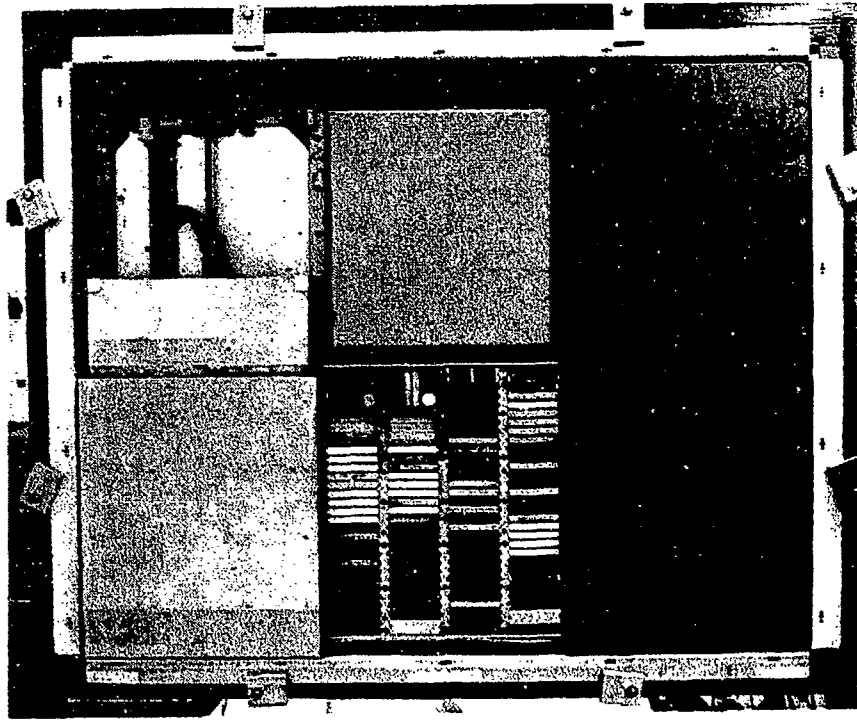


Figure 13. D4 tray postflight, before M0003 deintegration, in tray-holding fixture



Figure 14. D8 (LE) canister in open position, postflight. The two rows to the left (top to bottom in photo) were exposed for 9 and 19 weeks, respectively. The remaining test articles were exposed for 40 weeks

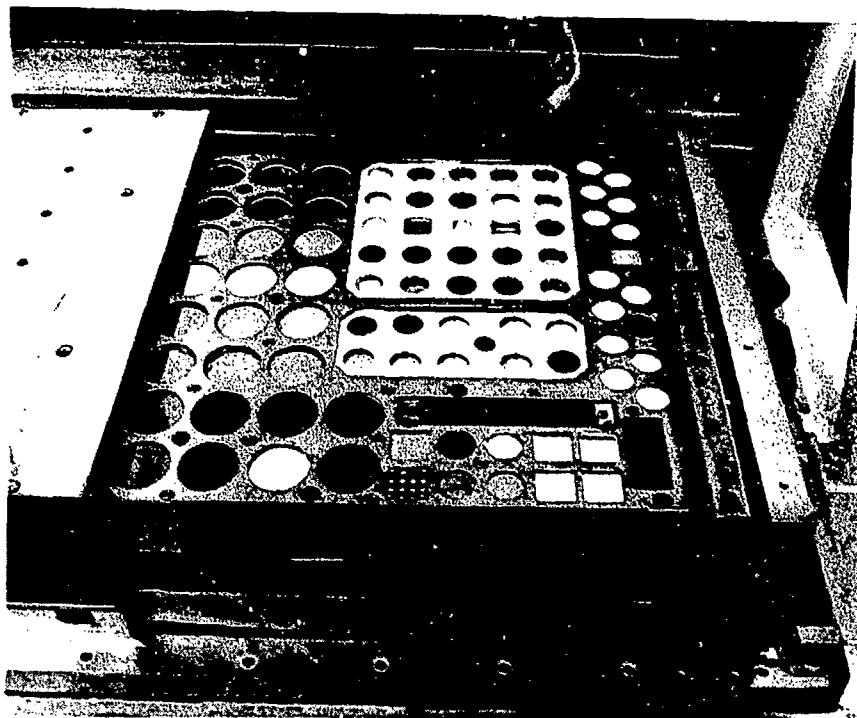


Figure 15. D4 (TE) canister in open position, postflight. Exposure was identical to that for D8 canister. Many, but not all test articles are duplicates of those flown on LE canister

Data Collection Timing

- SCAN OFF period after initialization
 - 2.333 hours
- Data collection sequence
 - 5 consecutive scans at 3.49 minute intervals
 - 32 intervals per sequence = 111.8 minutes
- Time between sequences
 - 93.16 hours
- SCAN runs to end of tape
 - approximately 429 days

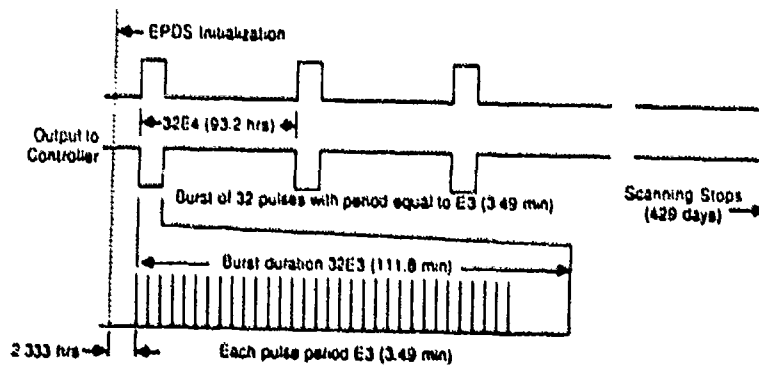


Figure 16. M0003 data collection sequence

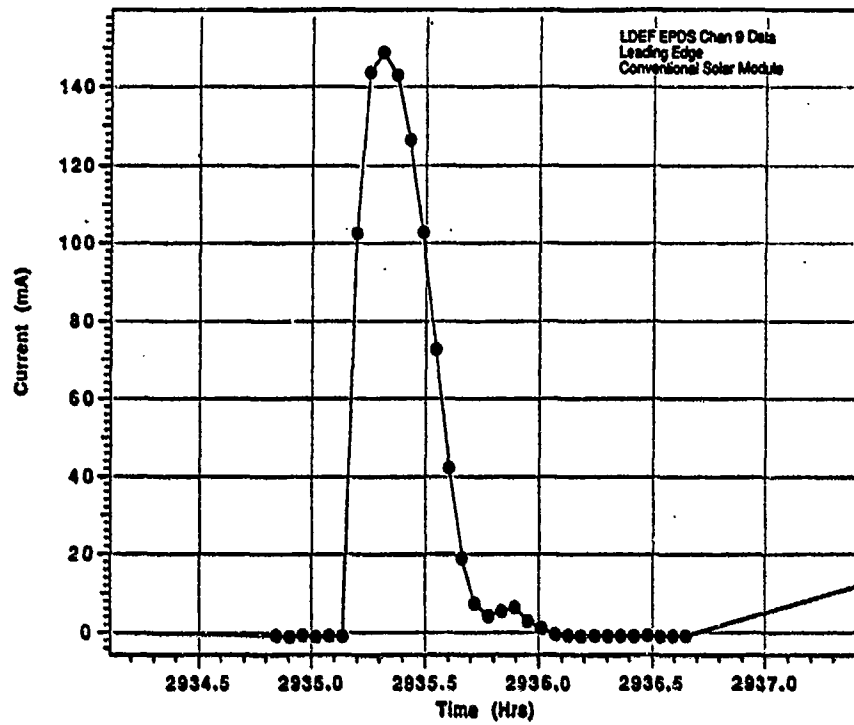


Figure 17. Typical orbital scan (111.8 min) data plot from conventional solar cell module

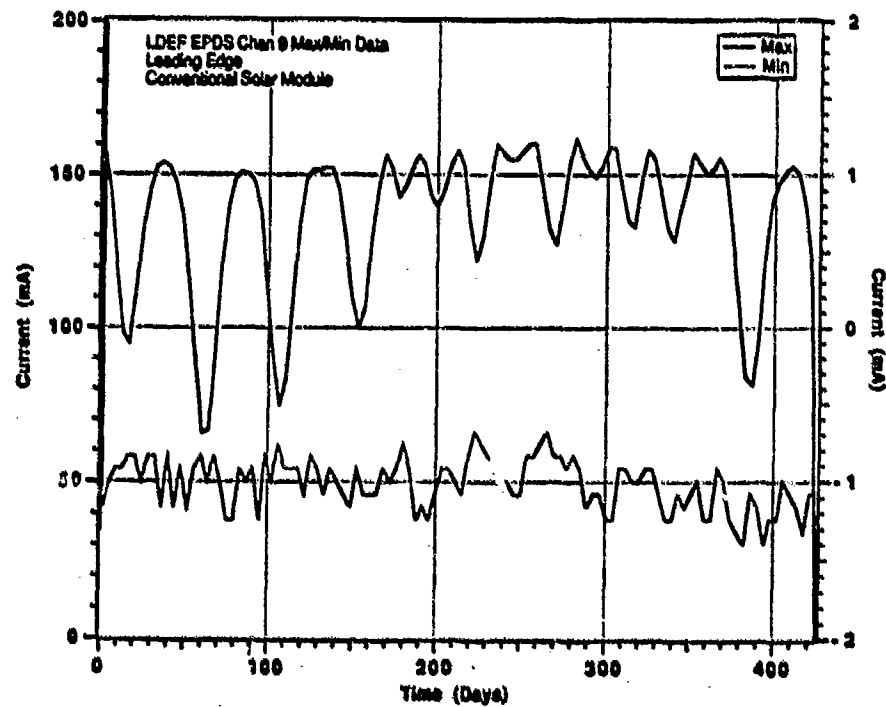


Figure 18. Min/max data plot for conventional solar cell data channel

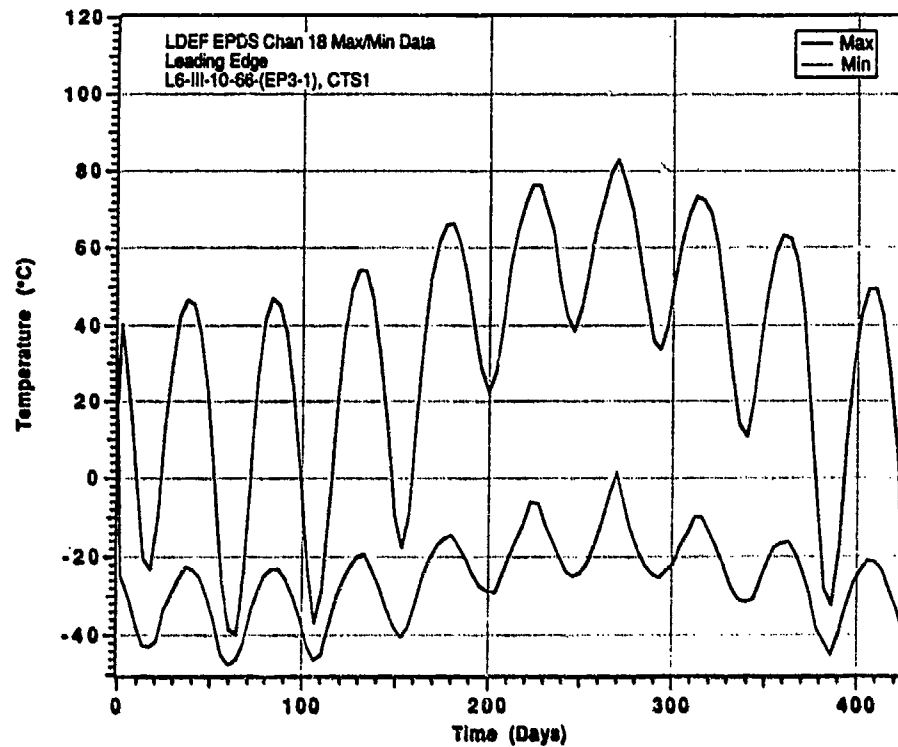


Figure 19. Min/max temperature plot for graphite-epoxy composite LE test article

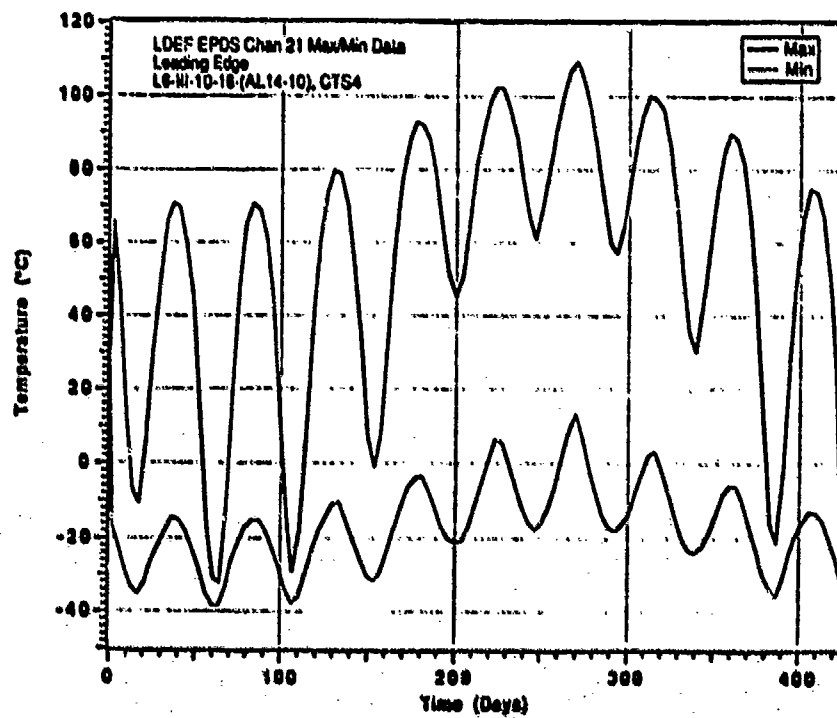


Figure 20. Min/max temperature plot for graphite-aluminum composite LE test article

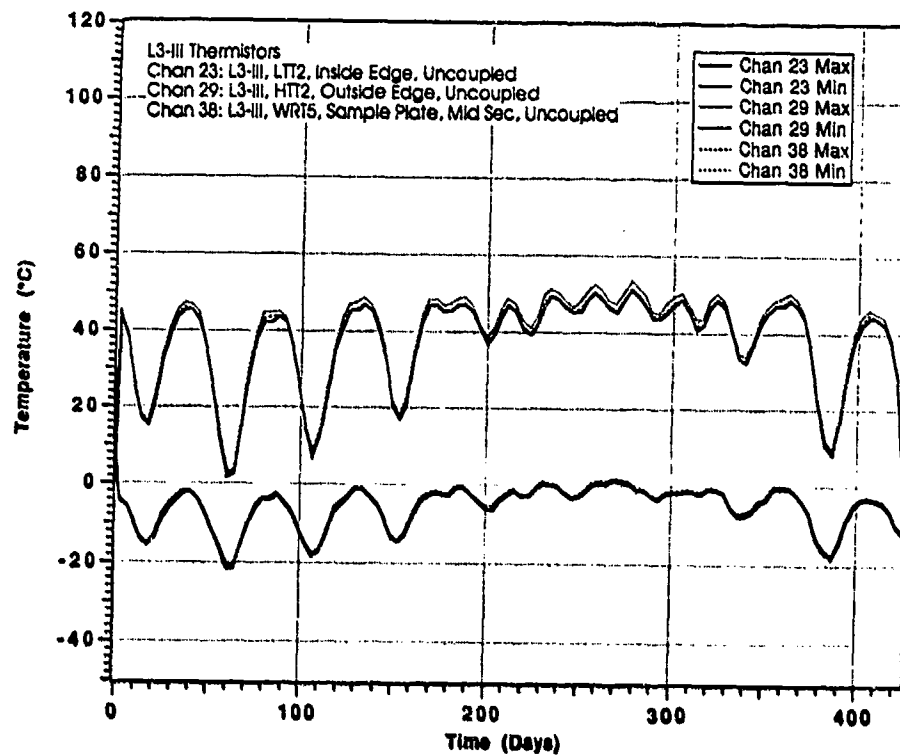


Figure 21. Thermal cycling plot for Module III on D9 (LE) tray

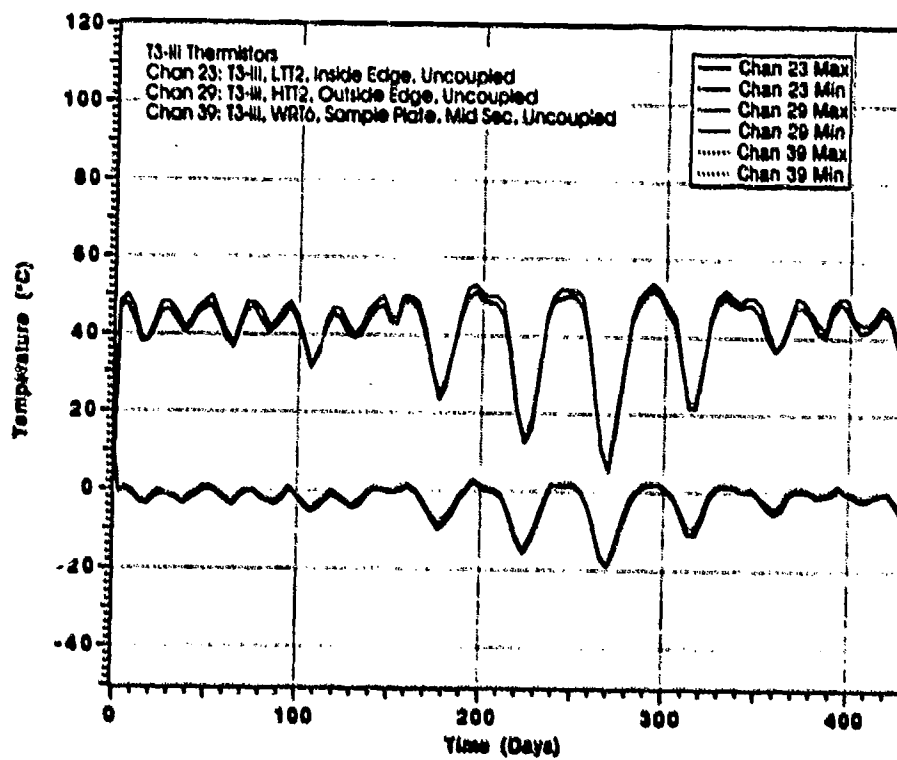


Figure 22. Thermal cycling plot for Module III on D3 (TE) tray

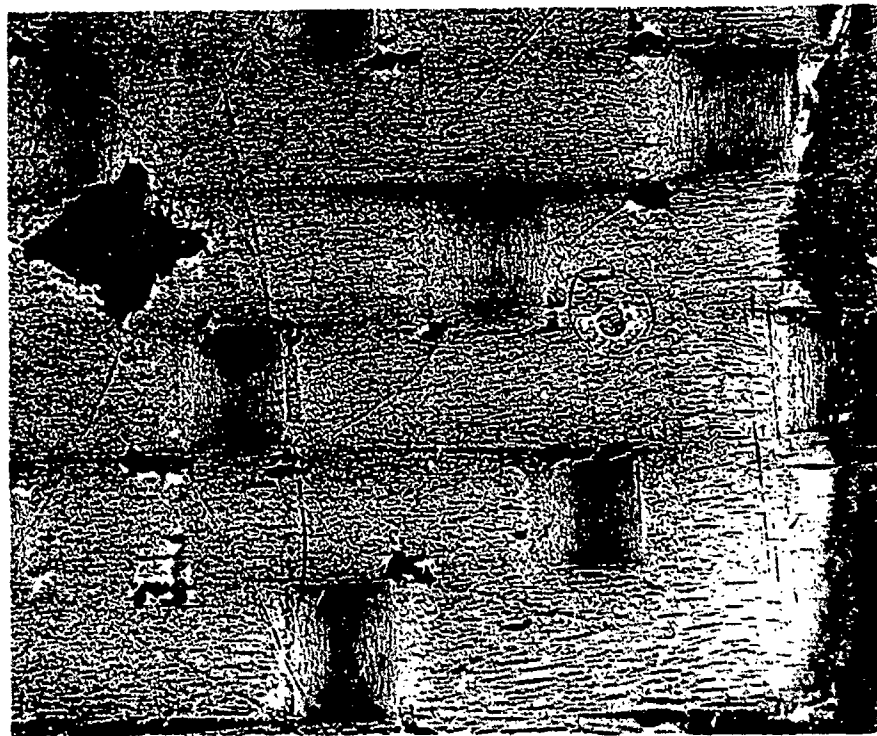


Figure 23. Atomic oxygen-eroded surface of graphite-epoxy composite test article exposed on D9 (LE). Note enlargement of impact crater, upper left. Masked, unexposed surface is at right edge of photo

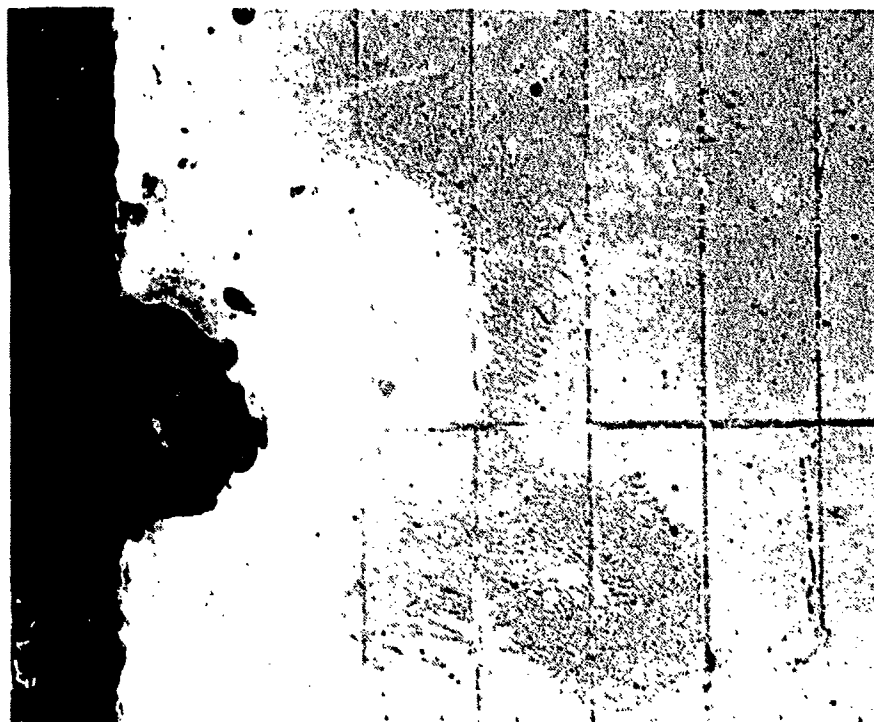


Figure 24. Localized delamination of cover glass near silver weld on LE solar cell

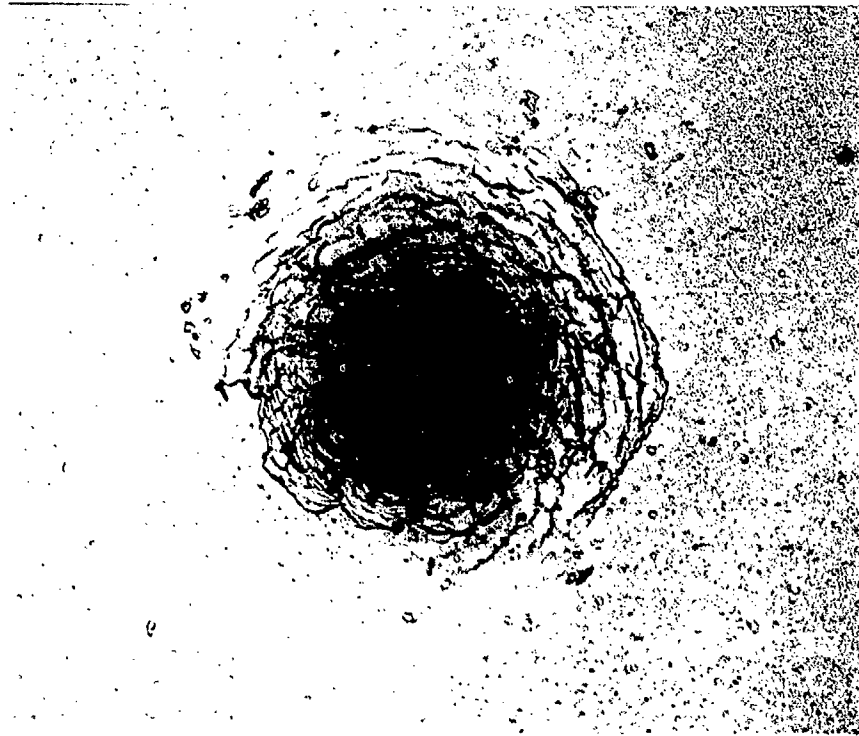


Figure 25. Typical micrometeoroid/debris damage in a solar cell cover glass

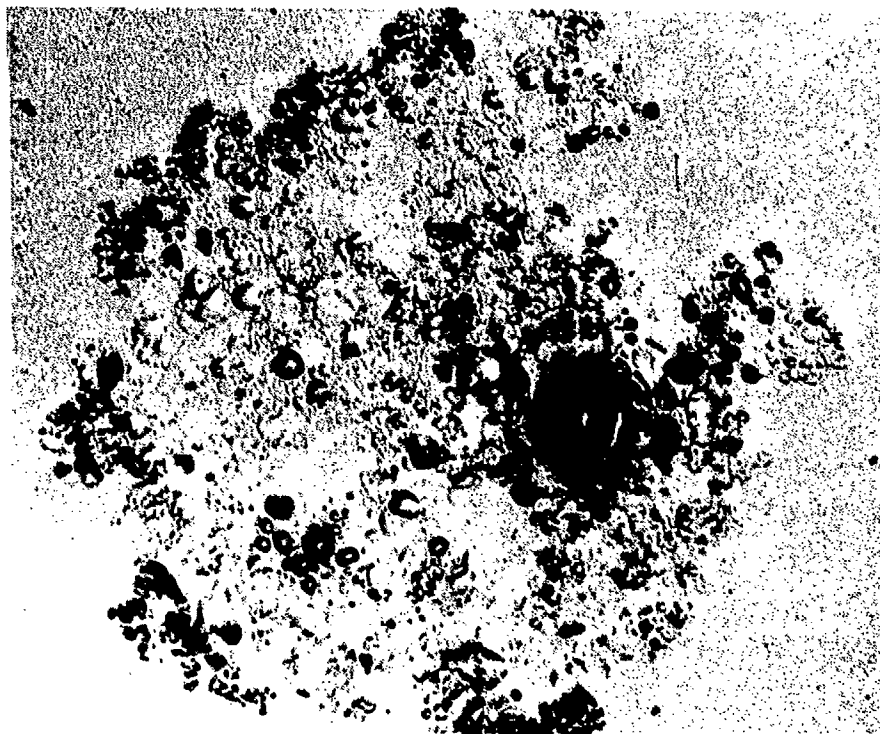


Figure 26. Blistered coating damage surrounding ~1-mm dia. impact crater in LE ThF₄/Ag/Mo mirror test article

Radar Camouflage Materials

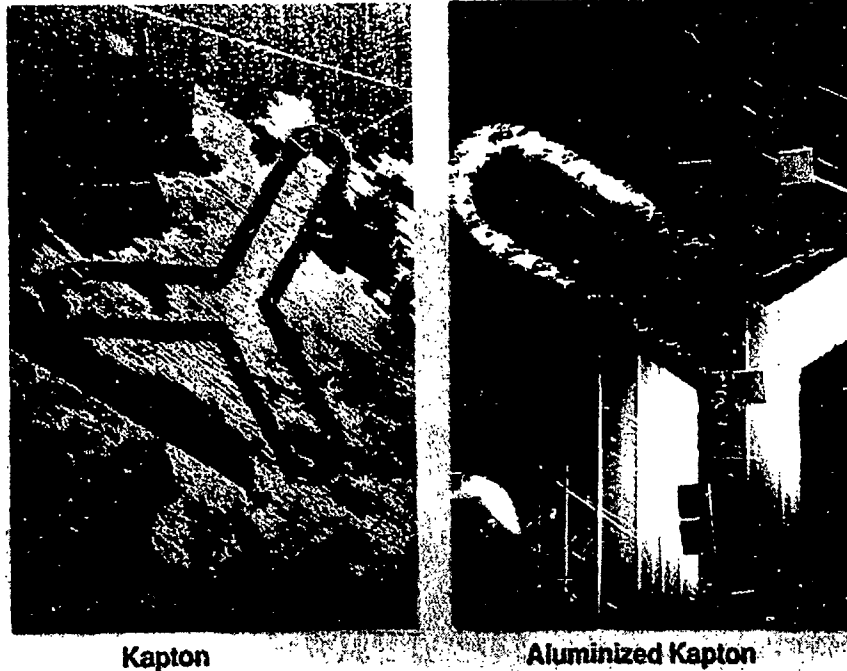


Figure 27. Atomic oxygen erosion of aluminized Kapton radar camouflage material. This produced significant debris which became scattered over many LDEF trays

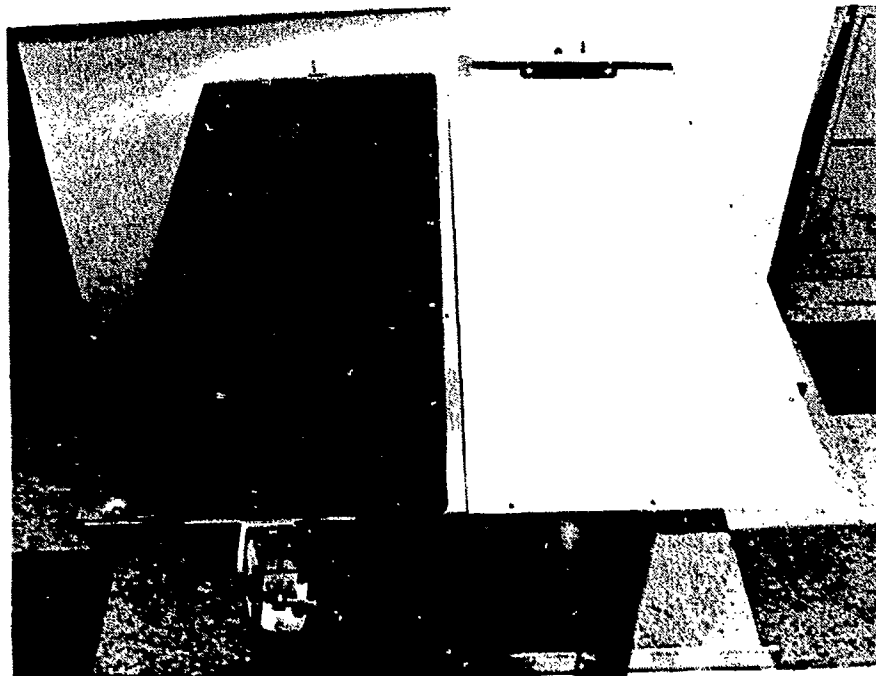
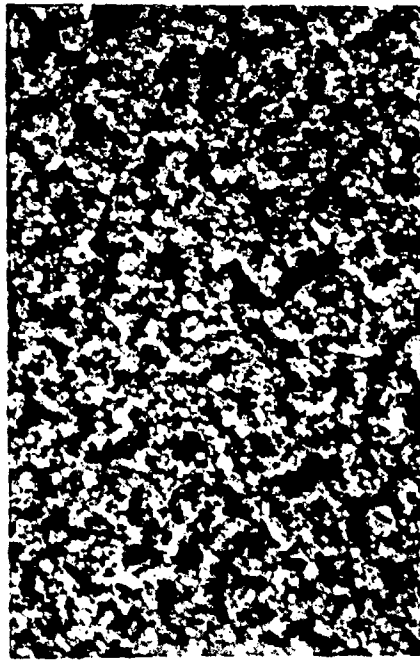
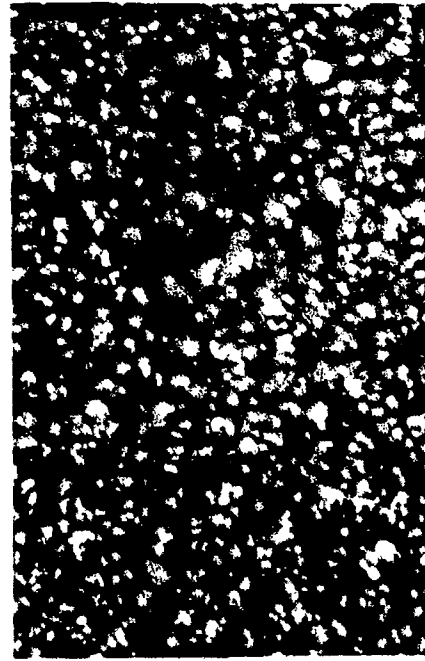


Figure 28. Chemglaze A276-painted sunshields flown on D4 (TE) on left and D8 (LE) on right

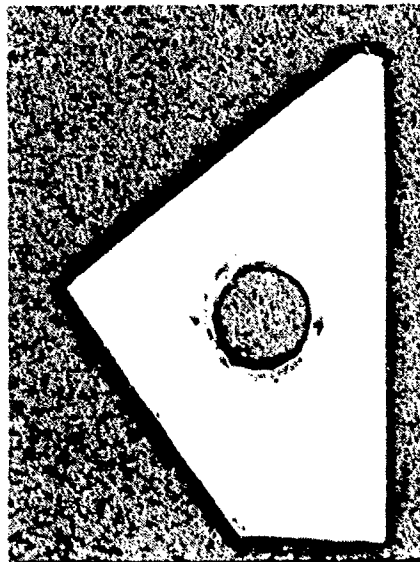


LEADING EDGE

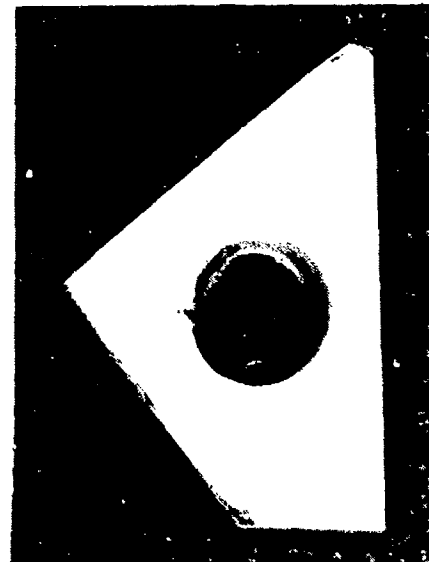


TRAILING EDGE

Figure 29. SEM micrographs of surface of Chemglaze A276 paint exposed on LE (left) and TE (right)



BEFORE UV EXPOSURE



AFTER UV EXPOSURE

Figure 30. Response of masked Chemglaze A276 to UV radiation

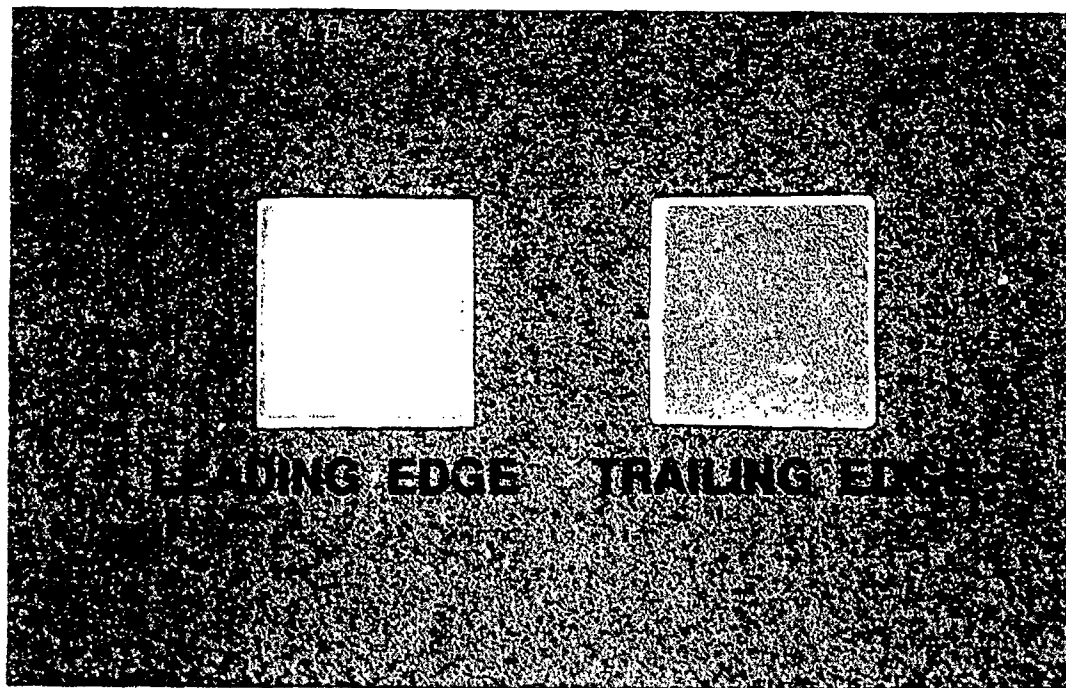


Figure 31. Side-by-side comparison of LE/TE S13GLO test articles

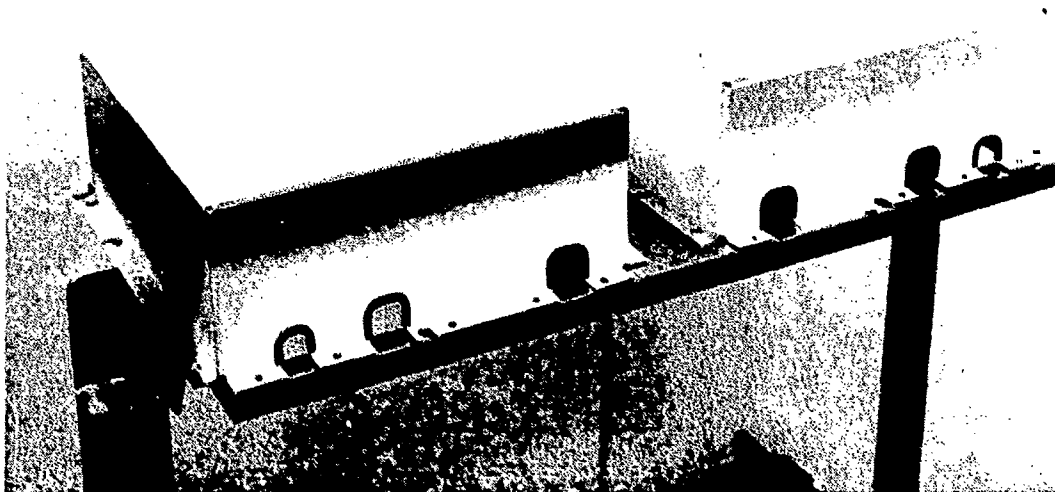


Figure 32. Signal conditioning unit (SCU) covers showing dramatic differences in damage from LE to TE. Note marked outgassing patterns on LE cover

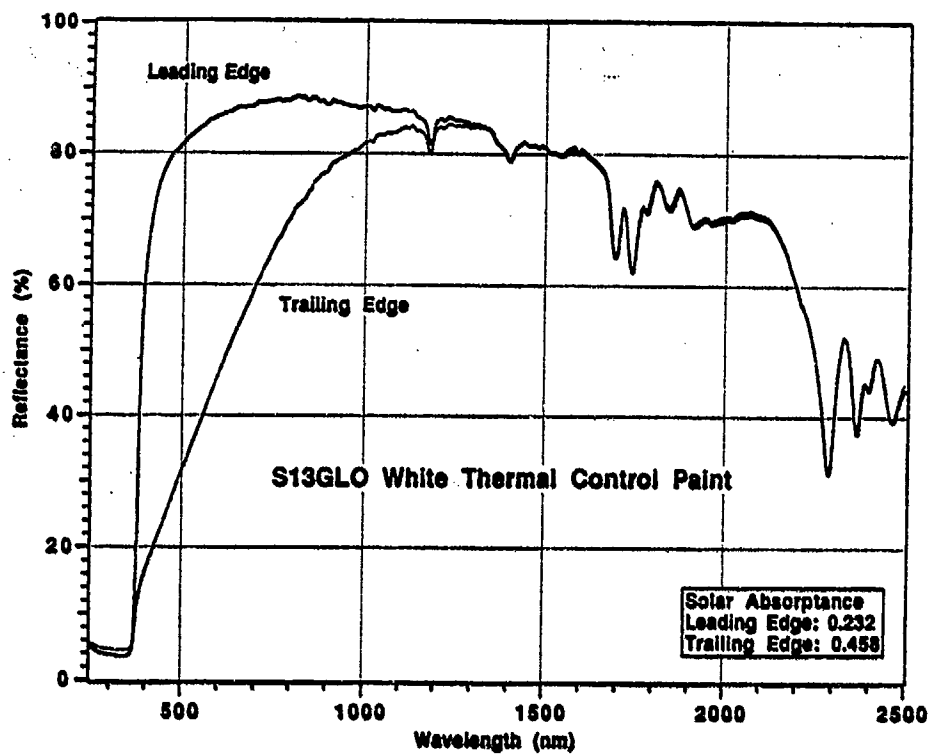


Figure 33. Reflectance curves for S13GLO

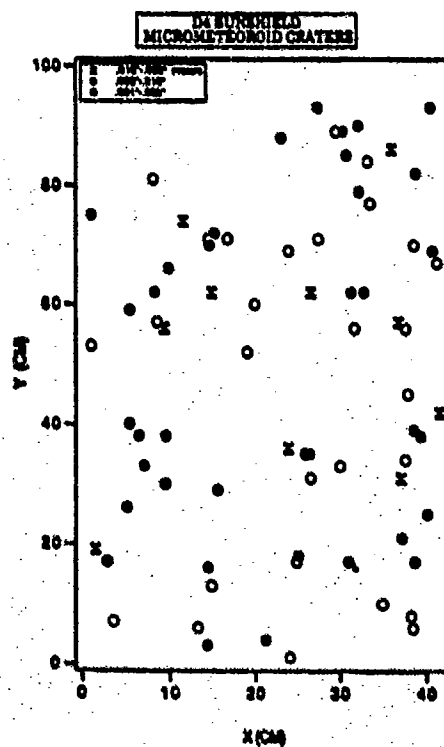


Figure 34. Micrometeoroid/debris impacts on TE EPDS sunshield

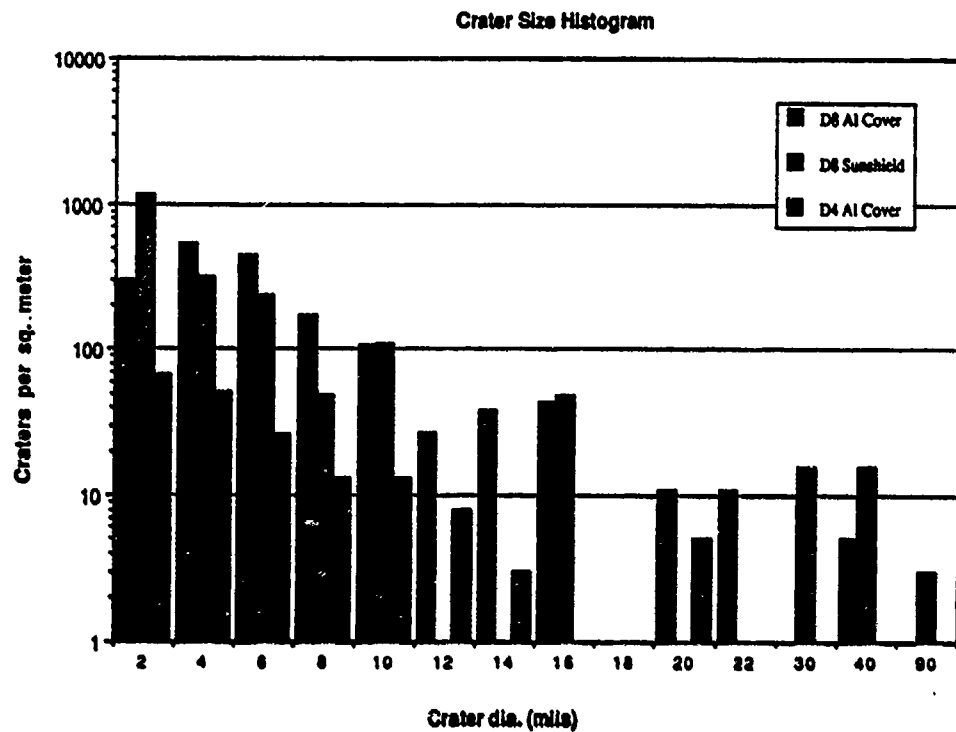


Figure 35. Histogram depicting micrometeoroid/debris counts for various D4/D8 surfaces



Figure 36. Puncture and impact crater in Chemglaze A276-painted EPDS sunshield on LE. The 2.5-mm dia. puncture is through 40 mil aluminum. Smaller impact is surrounded by zone of ruptured, eroded coating



Figure 37. Impact crater (1.25 mm dia.) in glass test article



Figure 38. Hypervelocity impact on embrittled surface of vacuum-distilled black RTV 602

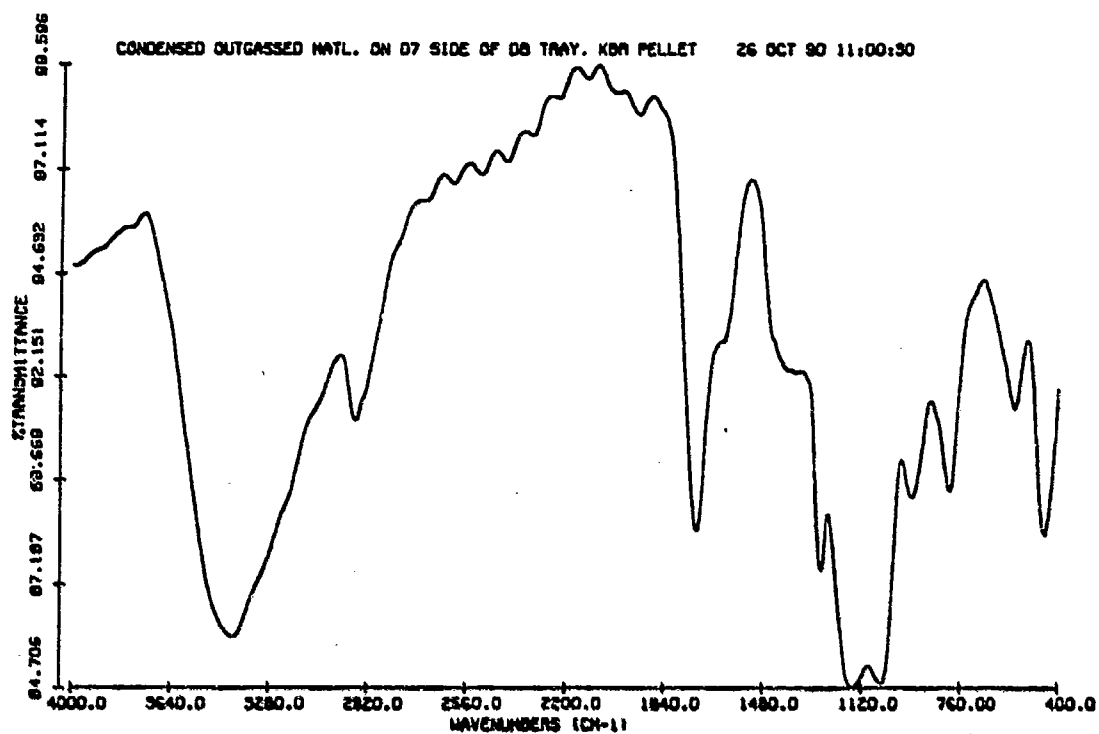


Figure 39. FTIR spectrum of varnish-like deposit on LE (D8) tray

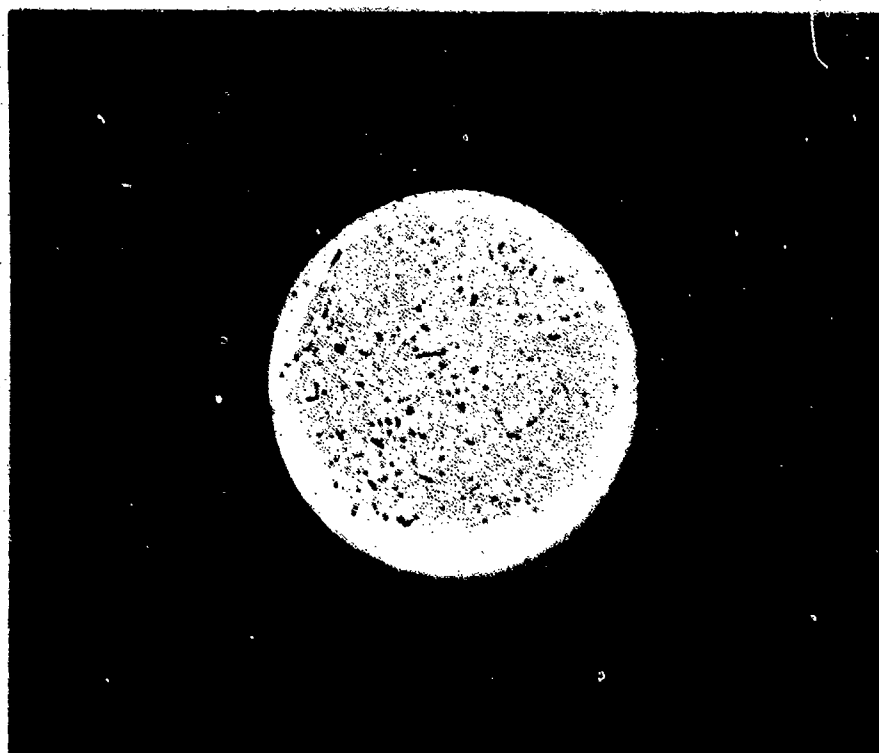


Figure 40. Debris contamination adhered to surface of 1.5 in. dia. silicone-based white paint test article exposed for 40 weeks in the TE (D8) canister